ANALYSIS AND DESIGN OF SLOW WAVE STRUCTURE FOR BACKWARD
WAVE OSCILLATORS

A THESIS SUBMITTED TO
THE GRADUATE SCHOOL OF NATURAL AND APPLIED SCIENCES
OF
MIDDLE EAST TECHNICAL UNIVERSITY

BY

DOĞANCAN ESER

IN PARTIAL FULFILLMENT OF THE REQUIREMENTS
FOR
THE DEGREE OF MASTER OF SCIENCE
IN
ELECTRICAL AND ELECTRONICS ENGINEERING

JANUARY 2019

Approval of the thesis:

ANALYSIS AND DESIGN OF SLOW WAVE STRUCTURE FOR BACKWARD WAVE OSCILLATORS

submitted by **DOĞANCAN ESER** in partial fulfillment of the requirements for the degree of **Master of Science in Electrical and Electronics Engineering Department, Middle East Technical University** by,

Prof. Dr. Halil Kalıpçılar
Dean, Graduate School of **Natural and Applied Sciences**   ————————

Prof. Dr. Tolga Çiloğlu
Head of Department, **Electrical and Electronics Engineering**   ————————

Prof. Dr. Şimşek Demir
Supervisor, **Electrical and Electronics Eng. Dep. METU**   ————————

Examining Committee Members:

Prof. Dr. Sencer Koç
Electrical and Electronics Engineering, METU   ————————

Prof. Dr. Şimşek Demir
Electrical and Electronics Engineering, METU   ————————

Prof. Dr. Asım Egemen Yılmaz
Electrical and Electronics Engineering, Ankara University   ————————

Assoc. Prof. Dr. Özgür Ergül
Electrical and Electronics Engineering, METU   ————————

Assoc. Prof. Dr. Avni Aksoy
Accelerator Technologies Institute, Ankara University   ————————

Date : 31.01.2019

I hereby declare that all information in this document has been obtained and presented in accordance with academic rules and ethical conduct. I also declare that, as required by these rules and conduct, I have fully cited and referenced all material and results that are not original to this work.

Name, Surname: Doğancan Eser

Signature   :

ABSTRACT

ANALYSIS AND DESIGN OF SLOW WAVE STRUCTURE FOR BACKWARD WAVE OSCILLATORS

Eser, Doğancan

M.S., Department of Electrical and Electronics Engineering

Supervisor: Prof. Dr. Şimşek Demir

January 2019, 80 pages

High power microwave is an emerging area that finds different applications in radar, directed energy weapons, plasma science, satellite communications, particle physics and medicine fields. Some examples of high power microwave devices are klystron, vircator, cyclotron, magnetron, travelling-wave tube amplifier (TWTA) and backward-wave oscillators (BWO). In this work, we focus on backward-wave oscillator that is one of the high power microwave sources. Backward-wave oscillator is a real high power microwave sources that convert electron beam energy to waves. It is also called as Cherenkov devices because emission process is analogous to Cherenkov radiation which occurs when the electron velocity exceeds the light velocity in that medium. Beam-wave interaction is achieved in the part called as slow-wave structure. Wave velocity is reduced below the electron beam velocity in this part. This part can be designed with periodic obstacles, dielectric or metamaterial. However, using dielectric is not preferred due to dielectric breakdown for high power microwave devices. Instead of that metallic periodic obstacles or metamaterials are used. This part affects the operation frequency, conversion efficiency, output power and compactness. As a

result of these, slow wave structure is the crucial part of the BWO.

In this work, we analyzed and designed the slow-wave structure for high power backward-wave oscillators. First, the unit cell of the slow wave structure simulation is performed in terms of dispersion diagram using commercial 3D electromagnetic solver. Modes of the SWS are also investigated for both empty circular waveguide and SWS. Interaction impedance which is the parameter for conversion efficiency is extracted for the unit cell. Phase velocity and group velocity of the wave in this medium is also simulated. Eight unit cells are combined to measure the propagation of the wave in that structure. Combined 8 unit cells are fabricated and measured in terms of S parameters. This measurement validates the dispersion diagram of the unit cell since it resonates for the desired mode and frequency. Hot test simulation of the slow wave structure is also investigated using commercial 3D particle solver. In this simulation, annular electron beam is used and validated SWS is used for hot test simulation. In order to confine the annular electron beam analytical magnetic field is applied. At the end, we observed the operation frequency as the 2.49 GHz which is in the passband region of the validated SWS.

ÖZ

GERİYE GİDEN DALGA OSİLATÖRLERİ İÇİN DALGA YAVAŞLATICISI TASARIMI VE ANALİZİ

Eser, Doğancan

Yüksek Lisans, Elektrik ve Elektronik Mühendisliği Bölümü

Tez Yöneticisi: Prof. Dr. Şimşek Demir

Ocak 2019 , 80 sayfa

Yüksek güçlü mikrodalga uygulamaları son yıllarda radar, yönlendirilmiş enerji silahları, plazma bilimi, uydu haberleşmesi, parçacık fiziği ve tıp alanlarında bir çok uygulama alanı bulmuştur. Klistron, virkatör, kiklotron, magnetron ,yürüyen dalga amplifikatörü (TWTA) ve geriye giden dalga osilatörü (BWO) yüksek güçlü mikrodalga kaynaklarının bazı örnekleridir. Bu tezde yüksek güçlü mikrodalga kaynaklarından biri olan geriye giden dalga osilatörü üzerinde durulacaktır. Elektron enerjisini dalga enerjisine çeviren geriye giden dalga osilatörü bir mikrodalga kaynağıdır. Bu cihazlar aynı zamanda Cherenkov cihazları olarak da bilinmektedir. Bunun nedeni Cherenkov ışıması ile olan benzerliğinden gelmektedir. Elektron hızı aynı ortamda bulunduğu ışığın hızını geçerse Cherenkov ışıması meydana gelmektedir. Elektron ve dalganın etkileşim gösterdiği yerler dalga yavaşlatıcı yapısı olarak bilinmektedir. Çünkü bu yapılarda dalganın faz hızı elektron demetinin hızının altına düşer. Bu işlevi gören yapıları tasarlamak için periyodik olarak konan engeller, dielektrik veya metamalzemeler kullanılabilir. Dielektrik kullanımı dalga yavaşlatıcı yapısı için uygun olsa da dielektrik kırılımından dolayı yüksek güçlü mikrodalga kaynaklarında

tercih edilmez. Dielektrik malzeme yerine periyodik olarak eklenen metal engeller veya metamalzemeler olarak da bilinen yapılar kullanılabilir. Dalga yavaşlatıcı yapısı osilasyon frekansı, dönüşüm verimliliği, çıkış gücü ve kompaktlık gibi birçok parametreyi etkilemektedir.

Bu tezde geriye giden dalga osilatörleri için dalga yavaşlatıcısı tasarımı yapılmıştır ve bu yapı analiz edilmiştir. İlk olarak bir dalga yavaşlatıcı yapısının birim hücresinin dağılım diyagramının öngörümlemesi 3B elektromanyetik çözümü yapan bir yazılımda yapılmıştır. Boş bir dalga kılavuzundaki ve yavaşlatıcı dalga yapısındaki modlar incelenmiştir. Dönüşüm verimliliğini doğrudan etkileyen bir parametre olan etkileşim empedansı da yine aynı programda incelenmiştir. Tasarımın bu yapısında dalga negatif bir grup hızına ve elektron demetine yakın bir hıza sahip olması gerekir. Bu nedenle dalganın faz ve grup hızlarının öngörümlemesi 3B elektromanyetik tasarım programında yapılmıştır. Bu tasarımda dalgaların yayılımını ölçmek için 8 birim hücreden oluşan bir yapı birleştirilmiş ve üretilmiştir. Bu üretim dağılım diyagramının doğrulanmasında kullanılmıştır. Ölçümlerde rezonans frekansları ve modu öngörümlemelerle yakın çıkmaktadır. Dalga yavaşlatıcı yapısının elektron demeti içeren öngörümlemesi de ayrıca yapılmıştır. Halka biçiminde bir elektron demeti yavaşlatıcı dalga yapısının içerisinde gözlenmiştir. Halka biçimindeki elektron demetini bir arada tutmak için analitik manyetik alan uygulanmıştır. Son olarak 2.49 GHz frekansında osilasyon yapan bir geriye giden dalga osilatörü gözlenmiştir.

Anahtar Kelimeler: Dalga yavaşlatıcı yapılar,Geriye giden dalga osilatoru,Metamalzeme, Dağılım diyagramı, Etkileşim empedansı

to the memory of Turkish soldiers gone but never forgotten

ACKNOWLEDGMENTS

TABLE OF CONTENTS

LIST OF TABLES

TABLES

LIST OF FIGURES

FIGURES

LIST OF ABBREVIATIONS

ABK   Annular Beam Klystron

BWO   Backward Wave Oscillator

CAE   China Academy of Engineering

CHAMP   Counter-electronics High Powered Microwave Advanced Missile Project

CRM   Cyclotron Resonance Maser

FEL   Free Electron Laser

HPM   High Power Microwave

LHM   Left Handed Media

MILO   Magnetically Insulated Transmission Line Oscillator

NINT   Nortwest Institute of Nuclear Technology

NUDT   National University of Defense Technology

PIC   Particle in Cell

PPML   Plasma Pulsed-Power and Microwave Laboratory

RBWO   Relativistiv Backward Wave Oscillator

RPM   Recirculated Planar Magnetron

SWS   Slow Wave Structure

TWT   Traveling Wave Tube

CHAPTER 1

INTRODUCTION

High power microwave (HPM) devices are devices that can provide more than 100 MW power in the centimeter and milimeter wave range of frequencies between 1-300 GHz. At high power levels, vacuum tube devices are the only candidate since the solid state transistor can not provide sufficient power. It is an emerging area as a new technology. HPM devices have application areas in radar systems, directed energy weapons, satellite communications and medicine. There are different types of high power microwave devices such as magnetron, travelling wave tube amplifier, klystron and backward wave oscillator. They are different from solid state transistor and vacuum tube transistor since operation principle is different and microwave circuit is the crucial part of the system.

The basic operation of all high power microwave devices resembles each other. An electron gun is used to produce electron beam. This electron beam is guided by external magnetic field. Otherwise, electrons hit the wall of the microwave circuit repelling each other which result in lower efficiency for devices. Moving electron interacts with the electromagnetic waves and transfers their energy to electromagnetic waves. This interaction is called as beam-wave interaction and occurs in microwave parts of the high power microwave devices.

One of the high power microwave devices is the backward wave oscillator (BWO). It comprises of electron gun, slow wave structure (SWS), output antenna and applied magnetic field. Electron gun is the part of the microwave devices that provides electron beam in vacuum tubes. Emitted electron mechanism of the electron gun can be the thermionic emission or field emission. Emitted electrons guided by the magnetic field since the free electrons repel each other. BWO is also called as the O-type de-

vices since electrons move parallel to magnetic field. Moving electrons parallel to magnetic field transfers their energy to electromagnetic waves. The condition that electrons transfer their energy to electromagnetic wave is the synchronism condition. Phase velocity of the electromagnetic wave should be close the axial velocity of the electron to provide synchronism condition. This process resembles the Cherenkov radiation which occurs when the electron velocity exceeds the light velocity in that medium.

Beam wave interaction occurs in the slow wave structure part of the BWO. It is the crucial part of the BWO since it affects the parameters like conversion efficiency, operation frequency, compactness of the device. Phase velocity of the electromagnetic wave is reduced to the axial electron velocity in this part. Otherwise, synchronism condition can not be provided since the phase velocity of electromagnetic wave is greater than the speed of light in the empty waveguide. It makes the interaction impossible. Loading dielectric can be method to slow wave structure however it is not appropriate for high power microwave devices because of the dielectric breakdown. So, full metal structures are needed as slow wave structure. Metalic slow wave structures are the periodic obstacles that slow the phase velocity of the electromagnetic wave. There are different types of SWS. SWSs are classified as conventional and metamaterial slow wave structure in this thesis. Works before the metamaterial invention is considered as conventional slow wave structures and design includes the metamaterial approach is considered as the metamaterial slow wave structures.

In this thesis, operation principle of the BWO is investigated. First of all, unit cell of the SWS is designed in order to fit the TM mode dispersion diagram in between 2.4-2.5 GHz because lower S band can be accepted as sweet spot considering beam power transfer. In addition, electronic components may have slot which is suitable for wavelength in these freqeuncy to penetrate into the electronic components. Dispersion diagram of the unit cell is observed for lowest order modes. Assuming the beam wave interaction occurs with the TM mode under the strong axial magnetic field, SWS is designed to provide TM mode propagation. Combined 8 unit cells are simulated. TM mode propagation is observed for the complete SWS excited by the axial pin. In order to validate the TM mode propagation, combined SWS is fabricated and excited with the axial pin as in simulation. Fabricated SWS is measured in terms

of the S parameters. Passband is observed in between 2.43-2.72 GHz with the correlation of dispersion diagram. Validation of the SWS which is suitable for TM mode propagation is achieved by the measurements. In addition, SWS under the electron beam is simulated using the CST Particle Studio. Annular electron beam is used with DC electron emission model. Inner and outer radius of the beam are 5 and 2.2 mm. 2 T analytical magnetic field is applied to guide the electron beam. Phase space plot of the electrons is observed to investigate the velocity and energy of electrons. Finally, operation frequency of the oscillation is observed as 2.49 GHz. 10.7 MW peak power is achieved at the output of the BWO for 450 kV and 100 A electron beam with %23.8 peak efficiency.

Based on the above mentioned content, this thesis includes 5 chapters. The first part is the introduction part which defines the thesis content briefly. Second part is devoted to explain the previous work in literature. In addition to the work on BWO including both metamaterial based and conventional SWS, second chapter also includes works on other high power microwave sources such as TWT, klystron, magnetron. Third chapter gives theoretical background to design SWS. In the chapter four, CST solvers used in this thesis mentioned briefly. Design details and simulation results are also given in the forth chapter. Final chapter is devoted to give conclusion, future work. In conlusion, backward wave oscillator simulation is achieved for the 450 kV, 100 A electron beam under the 2 T magnetic field with %23.8 peak efficiency. Peak output power is observed as 10.7 MW and oscillation frequency is 2.49 GHz.

CHAPTER 2

LITERATURE REVIEW

2.1 High Power Microwave Devices

High power microwave systems are an emering area as a new technology. It is defined as systems that exceed the 100 MW peak power at the frequency range 1 GHz to 300 GHz [1]. It has many applications in radar systems, directed energy weapons, satellite comminications, medicine and laboratory sources for susceptibility and vulnerability testing of electronic systems. This subject is one of the hot research topic studied in United States of America, China, Russia,Western Europe, Japan, Taiwan, India, South Korea, and Singapore. In these countries, most of the research is devoted for high power microwave weapons.

The Counter-electronics High-Powered Microwave Advanced Missile Project (CHAMP) is a successful and contemporary example of HPM weapons. It is a joint concept technology developed by Boeing and US Air Force, Directed Energy Directorate at Kirtland Air Force Base. The aim of this project is to develop air-launched directed energy weapon to damaging electronic systems with electromagnetic pulse. This system is tested on October 2012 by Boeing [9]. Besides that, studies [12]-[15] are done in Plasma,Pulsed Power, and Microwave Laboratory (PPML) in University of Michigan for new device which is termed as Recirculated Planar Magnetron (RPM) [15]. Possible advantages of RPM for airborne applications are discussed in these studies. 3D printed plastic anodes electroplated and thermal sprayed with copper is discussed in [17] for RPM.

Northwest Institute of Nuclear Technology (NINT), National University of Defense Technology (NUDT), and China Academy of Engineering (CAE) are places where

5

working on HPM devices. Main research topics are on to increase the power efficiency, overcome to pulse shortening phenomenon, increase the pulse duration and operation in low magnetic field. Magnetically insulated transmission line oscillator (MILO) and Triaxial Klystron Amplifier studied in [18] and [19]. Relativistic backward-wave oscillator (RBWO) is studied in NINT [20]. Advantages of RBWO are high power efficiency, high output power and high repetition rate. Russia also revealed its microwave cannon [10] in Jun 2015, which is supposed to disable drones and warheads at a distance of up to six miles. In Japan, researches are continuing in the fields that are plasma heating by Gyrotrons, accelerators by Klystrons, and Free Electron Laser (FEL) [1].

The history of microwave vacuum tubes starts from the first microwave generation by German physicist Heinrich Hertz in 1888. Actually, Hertz helped to general acceptance of James Clerk Maxwell's theoretical observation that claims electromagnetic disturbance travels in the free space with velocity of light. Researches were expanded to make Maxwell's equations understandable by "The Maxwellians" who are George Francis FitzGerald (1851-11901), Oliver Lodge (1851-1940) and Oliver Heaviside (1850-1925) [11] . The interest in radio science in the 20th century developed rapidly. In 1930s, higher frequency operation is observed connecting the cavities to electrical circuits. The first Klystron is produced in 1937 by Russell and Sigurd Varian [21] and microwave tube was born. "Klystron" is an ancient Greek verb referring to the action of waves breaking against a shore. After that, activity in microwave tube area followed by the invention of Magnetron, Backward-Wave Oscillator(BWO) and Traveling Wave Tube (TWT) during World War II . In the 1950s, gyrotrons came into the literature as a new device as a result of the efforts to control thermonuclear fusion for energy production which requires a detailed understanding of the interaction between particles and waves. In the 1970s, solid state devices dominate research areas and researches on microwave tubes are curtailed. From 1990s to now, that has changed and high power microwave tubes appeared in the research area. Historical trends in HPM devices is summarized in the Figure 2.1
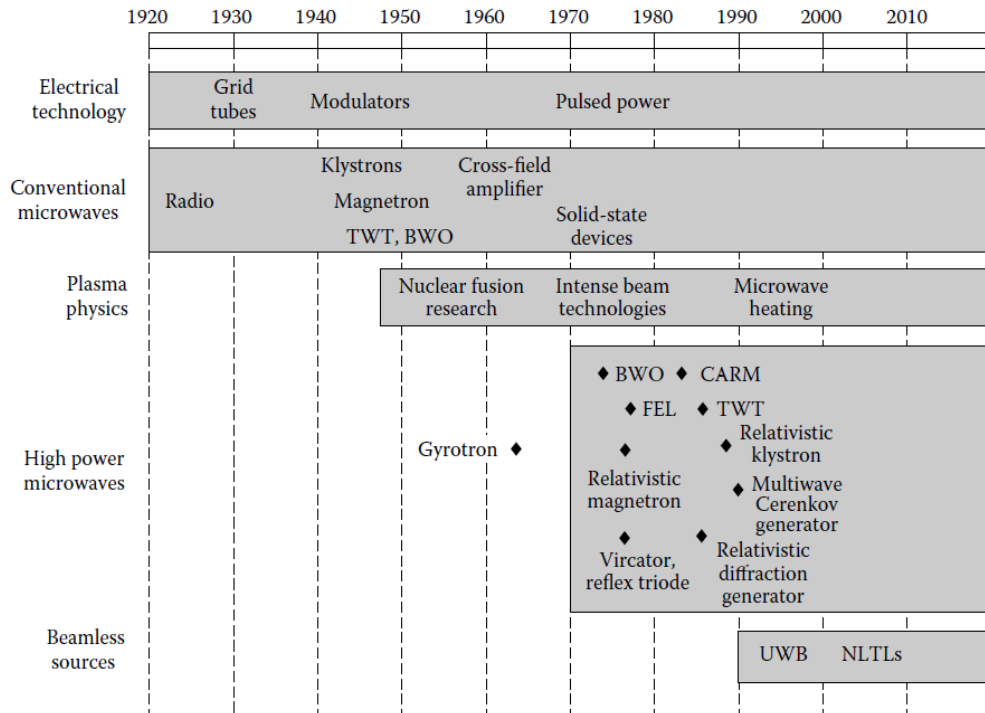
Figure 2.1: Historical origins and emergence of high power microwaves [1]

General components of HPM devices are prime power system, pulsed power system, microwave source and antenna shown in Figure 2.2. HPM devices need intense electrical pulses in the order of MV. This can be achieved by using capacitor banks that can store low voltage and slowly rising signal and provide high voltage, fast rising signal. Drivers part composed of prime and pulsed power system should be well-matched to microwave sources for efficient energy transfer. HPM devices show various impedance characteristics. This has been illustrated in Figure 2.3.
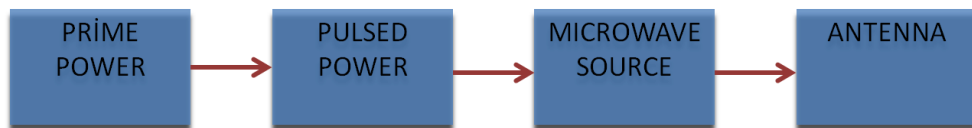
Figure 2.2: General Sketch of an HPM devices
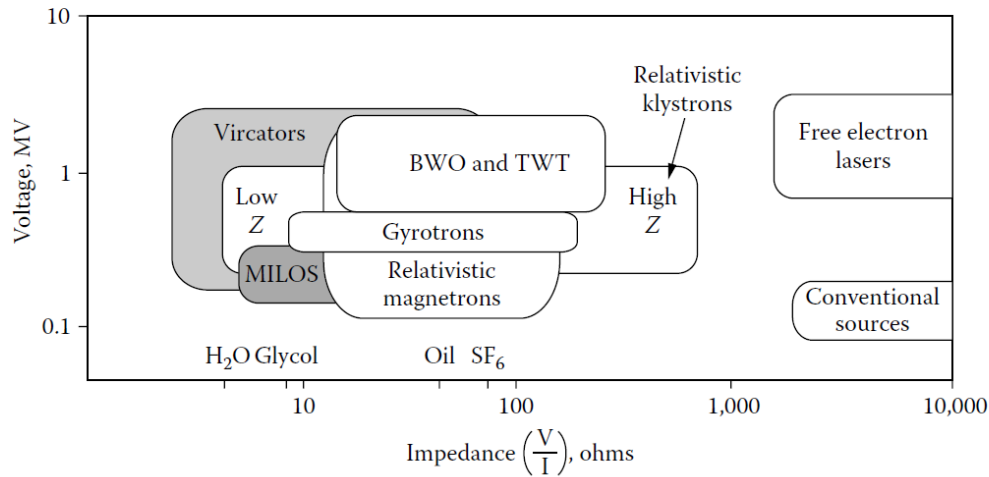
Figure 2.3: Various classes of HPM sources and conventional microwave sources with optimal impedance and voltage [1]

Driver parts are used to generate electron beam to provide electromagnetic radiation in microwave source part. There are three basic kinds of electromagnetic radiation by charged particles that are Cherenkov or Smith-Purcell radiation, transition radiation and bremsstrahlung [22]-[23]. Cherenkov radiation occurs when electron velocity is greater than phase velocity of electromagnetic waves. This type of radiation will be addressed in the next chapters. Transition radiation occurs when a charged particle passes through inhomogeneous media, such as a boundary between two different media. Klystrons are the examples for the HPM devices which transition radiation occurs. Bremsstrahlung radiation occurs when electrons oscillate in the external magnetic field or electric field. Cyclotron resonance masers (CRMs), free-electron lasers and vircators are the examples for bremsstrahlung devices. Alternatively, HPM sources can be classified into the 3 categories that are **O-type**, **M-type** and **space charge type**. For O-type devices, electrons move parallel to strong magnetic field. BWO and TWT are the examples for this type of device. For M-type devices, electrons drift perpendicularly to crossed electric and magnetic fields. Magnetron, MILO are the examples of the M type devices. In the last case, current exceeds the space charge limit and formation of virtual cathode is observed. Vircator is a good example to understand the radiation principle of this type of devices. Klystron, magnetron,

8

vircator, gyrotron and electron cyclotron maser, TWT and BWO are some of the examples of high power microwave devices.

Klystron is an O-type devices which composed of electron gun, drift tube and collector. Schematic representation of klystron is seen in Figure 2.4 . The basic idea behind the klystron is as follows. RF input signal is coupled to cavity with the same resonant frequency of the cavity fundamental mode TM_{010} . Depending of the phase of the fields excited by input RF signal, electrons passing through cavity are accelerated or decelerated by electric fields in the cavity. This results in bunches formation in the beam and it travels along drift tube. To guide the beam axial magnetic field can be applied along drift tube. Drift tube is designed to satisfy that electromagnetic modes are in cut off propagation between cavities. It provides the communication between cavities is made by only electron beam. Additional cavities enforce the bunching formation in the cavities at the excited field frequency. Then, high power output signal is extracted from the extraction cavity [1] and [24]
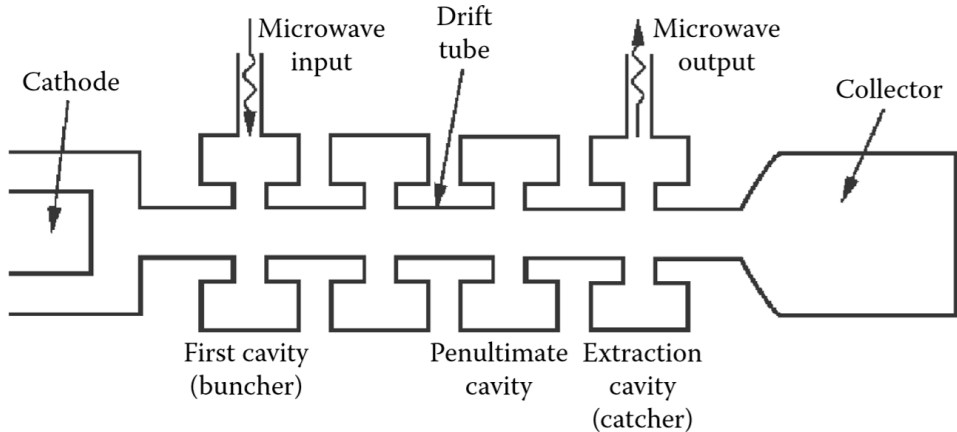
Figure 2.4: Schematic form of Klystron [1]

Klystron has been developed by L3 electron devices, Thales, Toshiba, Communications & Power Industries (CPI). Klystron has 12 MW peak output power with % 45 efficiency is developed at the 805 MHz by L3 Electron devices [25]. Toshiba (now Canon) is also another klystron manufacturer [26]. Thales is another manufacturer of the klystron[27]. Also, klystron research is going on in different bands. In the L band,

9

10 MW annular beam klystron (ABK) is studied in [28]. Triaxial klystron amplifier is demonstrated in the X band [29]. In the W band, klystron with 3D particle-in-cell (PIC) simulation is studied [30].

Magnetron is another high power microwave devices. Unlike the klystron, magnetron is a M-type Cherenkov devices which means it utilizes crossed electric and magnetic fields in order to generate microwave signal. Collins defines a magnetron as an EM wave-producing diode with the help of magnetic field [31]. It can be considered as a diode because of anode cathode structure. Negative voltage is applied to cathode of the magnetron. Cathode starts to emit electron through anode in the cathode anode region which is termed as interaction region. Electrons emitted from cathode move directly through anode when no magnetic field exists. If magnetic field perpendicular to electric field applied in interaction region, electron cloud around cathode can be created. Electron cloud in interaction region interacts with RF fields in the cavities. These cavities are analogous to parallel LC resonant cavity and determine the oscillation frequency. Example of the 3D model of magnetron is illustrated in Figure 2.5 .

Magnetron is produced in different companies. L3 electron devices have several models such as L127S which operates 2.625 GHz and can supply 750 kW and L4339A is a model at Ka-Band [33]. Toshiba is another company among magnetron manufacturer [34] . For high power applications such as linear accelerator, GLVAC is designer and manufacturer [35]. There are several research on magnetron in terms of simulation, stability of operation, phase controlling etc.. Magnetron simulation requires beam wave interaction solution which is possible with particle in cell (PIC) solver. Multiphysics simulation of a magnetron which means electrical, magnetic, thermal and mechanical characteristics with CST STUDIO SUITE is studied in [32]. X band magnetron with 8 cavities is simulated using three configurations of the CST software which are Eigen-Mode, PIC solver and Particle Tracking [36]. Comprhensive study on simulation of magnetron with CST software is published by Türker and Yeğin [37]. Stability of the oscillation frequency is another issue for the magnetron and investigated in [38]. Phase controlling in magnetron is investigated in [39] - [40].
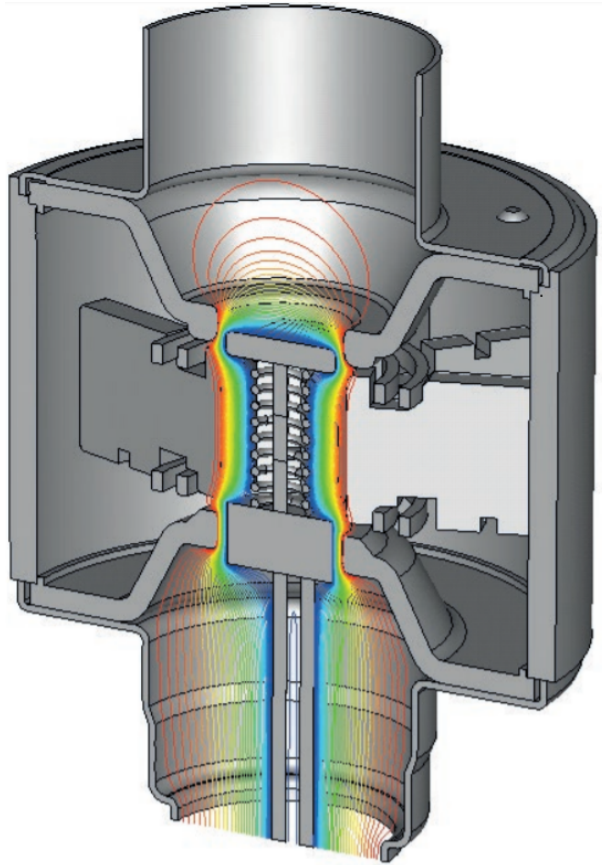
Figure 2.5: 3D Modeling of Magnetron [32]

Traveling wave tube amplifiers are one of the high power microwave devices which have wide variety of applications. TWTs account for over 50% market area of all microwave vacuum tubes [44]. TWTs are also termed as O-type devices since they utilize axial magnetic field to focus the electron beam generated by electron gun. As in other microwave vacuum tubes, TWTs operation principle is also based on beam wave interaction phenomena. Electron gun is used to generate electron beam. Axial magnetic field provided by permanent magnet or coil ensures to guide electron beam. This prevents the scattering of electrons by repelling each other. Input RF signal is applied to drift tube part as shown in Figure 2.6. Drift tube part ensures to equalize the phase velocity of microwave signal to the speed of electron to provide synchronism condition. Drift tube part is also called as slow wave structure since it slows the phase velocity of electromagnetic wave. It is important part for efficiency of TWT. Output signal is extracted from the RF output port as shown in Figure 2.6. Electrons passing

drift tube is collected in the multistage depressed collector or just called as collector. This part is also subject for ongoing research to increase efficiency. Commercial TWTs are available in different companies. L-4920 provides 175 kW peak output power with 40% electronic efficiency requires 40 kV are one of the product of L3 Electron devices company which operates in the 420-450 MHz band [42]. Also, Communications & Power Industries has several products from C-band to Ka-band [43].
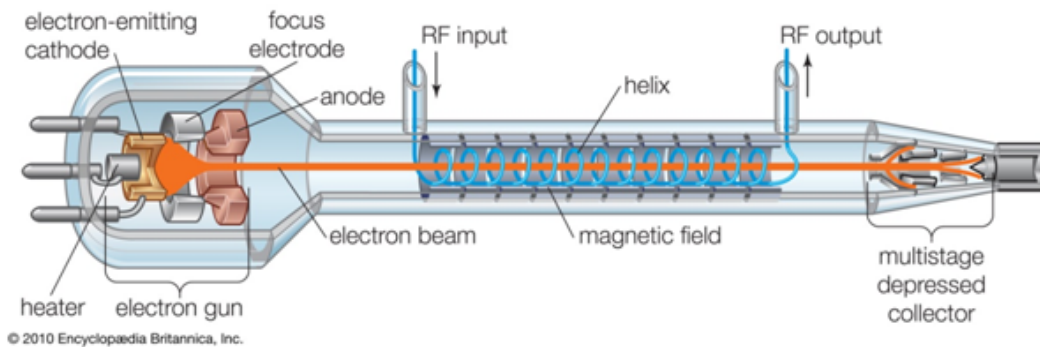
Figure 2.6: Schematic of TWT [41]

Conceptually, the electron gun, electron beam and collector are nearly same for all TWTs. However, differences are on RF circuits which are called slow wave structure. Most known examples of SWS part are composed of helix and coupled cavity. In this part, synchronous operation occurs when the velocity of the electron beam is made equal to the phase velocity of electromagnetic wave propagating in this medium. If the group velocity of electromagnetic wave is in the same direction with electron beam it is called forward wave. If wave has negative velocity, it is called as backward-wave which forms the basis of backward-wave oscillator. BWO will be the subject of the next section of literature review.

2.2 Backward-Wave Oscillators

Backward wave oscillator is one of the microwave vacuum electronic devices (MVED). It comprises of mainly 3 parts which are electron gun, slow-wave structure and output antenna. Output antenna can be changed with mode converter or collector to extract

the output power. Different configurations are shown in Figure 2.7 , 2.8 and 2.9. Although there are different configurations, operation principles are same for all BWO devices. Initially, electron beam is generated by the electron gun with electron emission such as explosive emission. Generated electron beam is guided with magnetic field in the SWS part since it repels each other. Kinetic energy of electron is converted to RF power with synchronism condition which requires to equalize the speed of electron and phase velocity of the wave in the SWS part. After the energy exchange is occurred in the SWS part, electrons are collected at the wall of output antenna that acts as collectors. Growing backward wave is reflected at the electron gun end and translate to forward wave through antenna. This process is explained in the [44] in detail.

Inventor of the BWO, R. Kompfner says that " The BWO is a kind of TWT; its invention was a natural consequence of the insights gained from the work on the TWT " [45]. He invented the BWO while working on TWT on 1951. Comprehensive study of theory of BWO is published by H.R.Johnson in 1955 [46]. Years later, 15 MW output power with 0.05 % conversion efficiency is observed as a result of interaction of the relativistic electron beam to slow wave structure in the Cornell University [47]. High power backward wave oscillator is constructed by relativistic electron beam generator operates with 750 kV, 3.3 kA [48]. Comprehensive study on BWO with rippled wall is investigated in [49] with 20% efficiency .As highlighted above, main BWO operation is based on the conversion of beam energy to wave. Key area of researches is on to increase the conversion efficiency of the BWO. The reason behind that efficient device does not need to high voltage and current to provide same output power which means smaller prime power source. Besides that, smaller current indicates the reduction in the magnetic field since the space charge effects reduce. All of these reduce the overall size of the device. Research on BWO after 1990 is the subject of the next sections. Slow wave structures which are designed before the metamaterial and is not designed with negative permittivity and permeability will be the subject of the conventional SWS. Others are the subject of the metamaterial SWS.
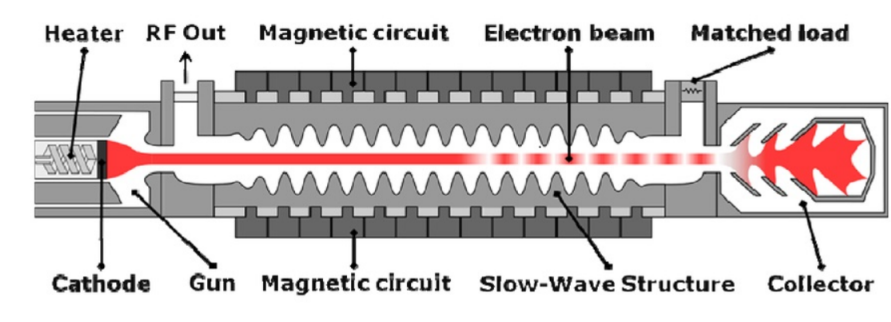
Figure 2.7: Schematic of BWO with end collector configuration [50]
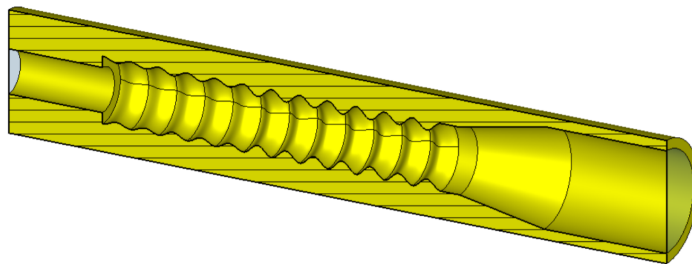
Figure 2.8: Schematic of BWO with output horn antenna [51]
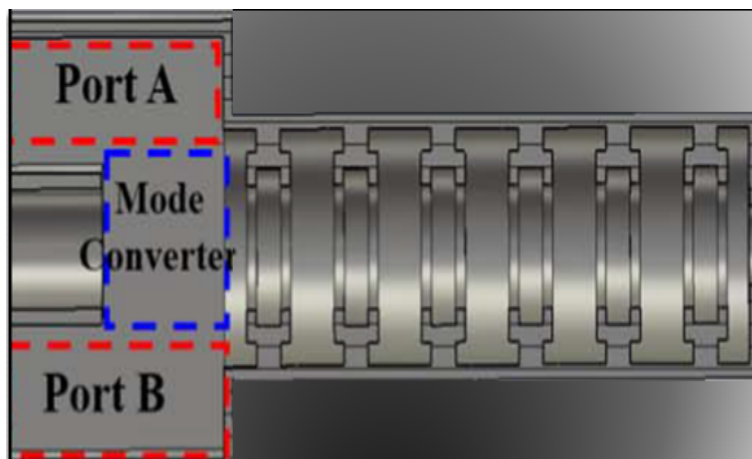
Figure 2.9: Schematic of BWO with mode converter [52]

2.2.1 Conventional Slow-Wave Structure BWO

Sinusoidally corrugated slow wave structure is the one of the most known type of the SWS. Sinusoidal corrugation can be uniform or nonuniform amplitude variations. Generally, nonuniform amplitude is used to increase the efficiency of the BWO. Trapezoidal, solid rectangular corrugation are also types of the corrugation. Theory of the relativistic BWO with end reflections is investigated with sinusoidally carrugated slow wave structure in [52] as in Figure 2.10. Although there are number of experiments reported in this area, it is the theoretical explanation of the operation of BWO with end reflections. Efficiency enhancement of BWO using nonuniform sinusoidally corrugated slow wave structure is investigated in 1994 by Edl Schamiloglu [53]. They reached 550 MW output power at 9.45 GHz in an 8-ns pulse with 22% electronic efficiency. Nonuniform ripples are used as SWS shown in Figure 2.11.
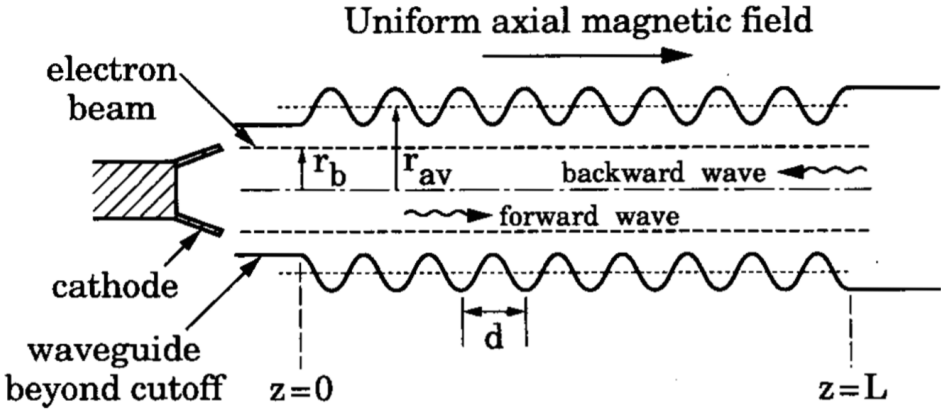
Figure 2.10: Sinusoidally Corrugated SWS [52]
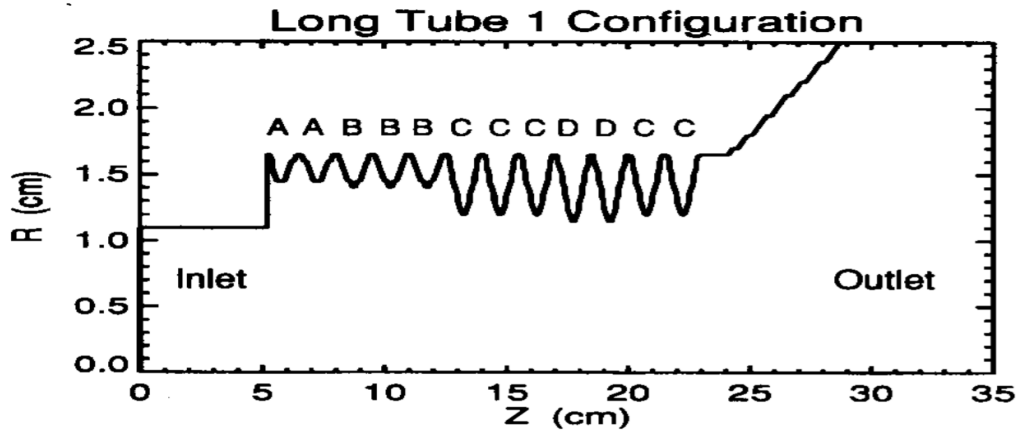
Figure 2.11: Nonuniformly Corrugated SWS [53]

Experimental studies on relativistic BWO with sinusoidally corrugated is published in 1998 [54]. BWO generated 200 MW output power with 4% efficiency in experiment. From sinusoidally corrugated SWS, trapezoidal corrugated SWS is observed in X bant [55]. Also, corrugation in wall can be rectangular solid as in [56]. Researches are also going on THz range with the same type corrugation [57].
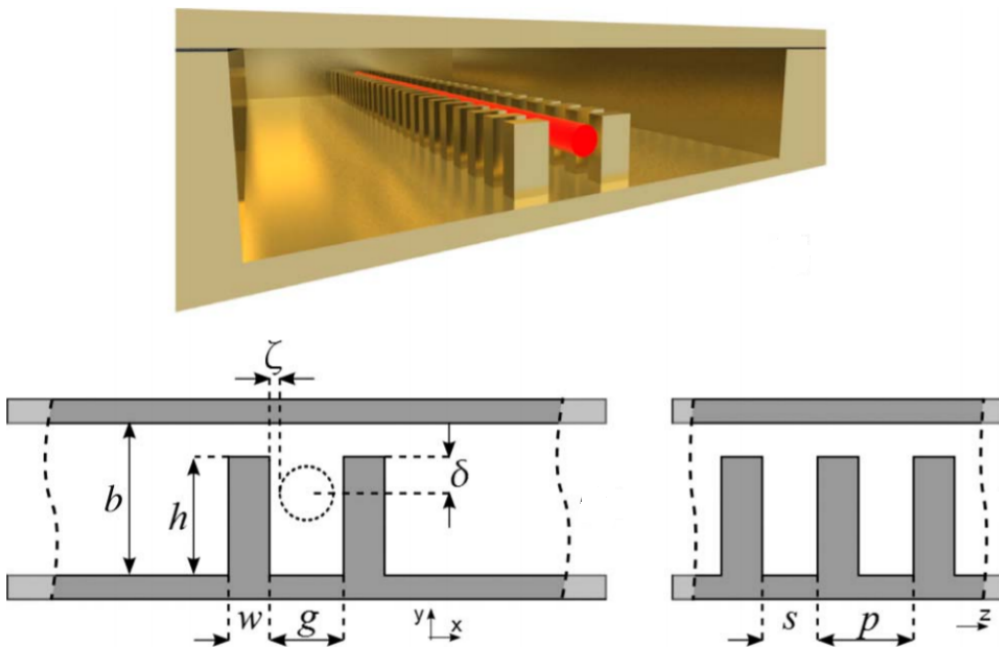
Figure 2.12: Rectangular Solid Corrugation SWS [57]

16

All of the aforementioned SWS can be classified as rippled wall SWS. Besides that coupled cavity SWS is also in the literature. Although it used in TWT, it can also be candidate for BWO operation [58]. Helix slow wave structure is also well-known type of the SWS. These structures are designed analytically or numerically. Conventional SWS has also similar properties with metamaterial SWS in terms of lowest order propagating waves is below the cutoff in smooth-wall waveguide, low-order slow waves can show the negative dispersion [59]. Therefore, vacuum tube workers were studying metamaterial properties without knowing it. SWS designed after the appearance of metamaterial and includes the metamaterial approach will be the subject of the next section.

2.2.2 Metamaterial Slow-Wave Structure BWO

With the publication of Vesellago in 1964 [60], lots of research have been done on artificial materials. He showed the possibility of wave propagation in medium with negative permittivity and permeability for some radian frequency ω. He termed these materials as left handed media (LHM) since wave vectors $\vec{k}$ is the left handed triplet of the electric field vector $\vec{E}$ and magnetic field vector $\vec{H}$. Besides that supporting the negative refractive index, reversed Doppler effect and reversed cherenkov radiation are exotic properties of metamaterials [61]. Also LHM can support a strong axial electric field component due to the strong resonance [62] . Since the BWO is an O-type Cerenkov radiation based device, metamaterials take place in research area supporting this property.

In 2010, cold simulation of the metamaterial SWS is done in MIT using high-frequency structure simulator code [63]. Hot test simulation is done with 500 keV, 80-A electron beam in CST Particle Studio. Dispersion diagram is simulated and beam line is observed on the same plot. The frequency of the negative index TM mode excitation is predicted in 2.65 GHz while the operation of the BWO is 2.595 GHz with 80-A electron beam. Coupling impedance is found as 46 Ω. Output power is observed 5.75 MW with 14 % efficiency. Same group published an article in 2016 with experimental results [64]. They observed 5 MW at 2.40 GHz. In this article they also considered the Cherenkov-cyclotron instabilities [65] in addition to Cherenkov radiation which

would lead to BWO interaction. In 2018, they made another experiment of BWO in [66] with reverse symmetry as shown in Figure 2.13.

The Schamiloglu group at the University of New Mexico studied the metamaterial based BWO in L band [67]. They used complementary split ring resonators and they achieved 95 MW at 1.43 GHz. Secondly, they reached 250 MW output power at 1.4 GHz. Split ring resonator is used as shown in Figure 2.14. The metamaterial SWS consist of two split ring resonator that are 180 complementary pair.
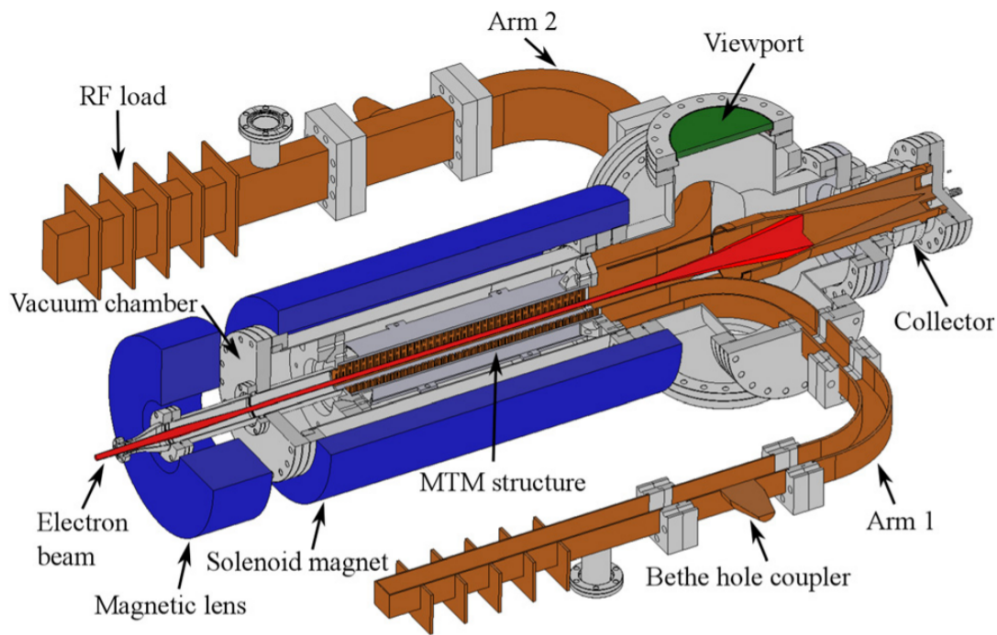
Figure 2.13: Schematic of Metamaterial based BWO [66]

Works on reversed Cherenkov radiation in left handed media started in 2007 at UESTC. They reported the electromagnetic properties of a waveguide loaded by complementary electric split ring resonator [69]. Negative permittivity and permeability is observed retrieving from the S-parameters. All-metal metamaterial is designed in [70]. They observed 4 MW peak output power with 31.5% efficiency at 2.454 GHz. In 2017, they simulated very high efficiency BWO with metamaterial in [71]. 20.7 MW output power is simulated with 92.4% electronic efficiency. Reversed Cherenkov radiation is observed experimentally in 2017 with the same group [72].
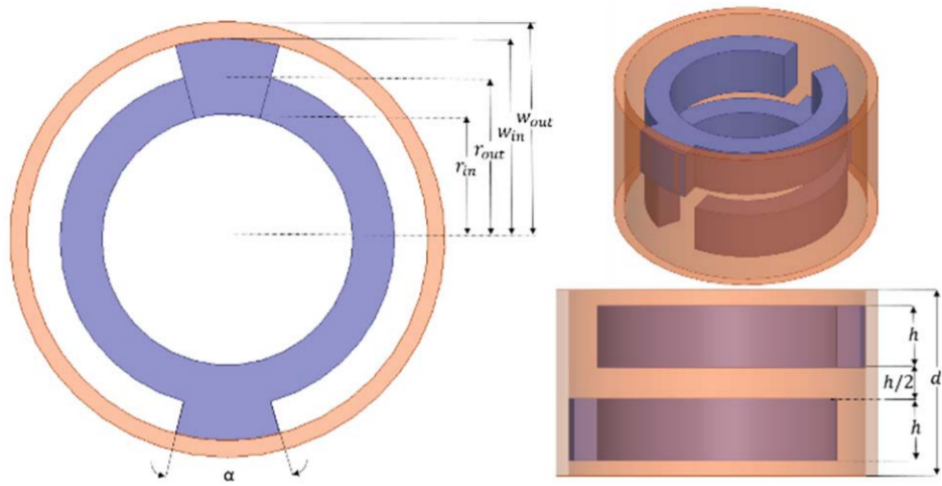
Figure 2.14: Geometry of Metamaterial SWS used in [68]

CHAPTER 3

THEORY OF OPERATION

Backward Wave Oscillators (BWO) are one of the high power microwave sources. As mentioned in the previous sections, operation principle of the BWO is based on the electron beam interaction with wave. BWO consists of electron gun which generates electron beam, slow wave structure, collector and magnetic field which guides the electron beam. In this work, the main interest is on analyzing metamaterial slow wave structure which is the crucial part of the BWO.

3.1 Modes on Circular Waveguide

A hollow circular waveguide supports TE and TM waveguide modes. Figure 3.1 shows the the geometry of the waveguide. In the analysis, cylindrical coordinates are used.
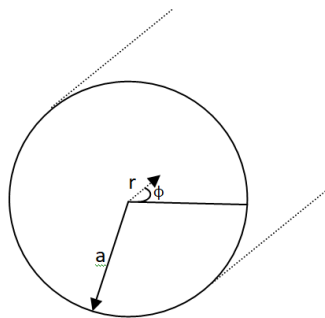
Figure 3.1: Geometry of Circular Waveguide

In this thesis, SWS is formed by waveguide below the cutoff frequency for TM mode. According to the [73], the permeability μ is negative when the TM mode propagation is possible for below the cutoff frequencies. Besides that, permittivity should also be negative in order to create propagation in bacward direction. Also, in order to create beam wave interaction, there should be axial electric field component which signs to TM mode. Considering all of these, only TM mode analysis of circular waveguide is investigated in this section. For TM modes, $H_z = 0$, and E_z is the solution of the wave equation. Wave equation is expressed in the equation 3-1 for axial electric field component. Here, it is worth the note that wave equation is an eigenvalue equation since the gradient operator does not change the direction of the electric field vector. Wavenumber is the eigenvalues and electric field vector is the eigenvector. CST Eigen Mode Solver will be used to identify the analysis of the mode in SWS and circular waveguide.

$$\nabla^2 E_z + k^2 E_z = 0 \tag{3-1}$$

For the TM modes of the circular waveguide, wave equation in cylindrical coordinates 3-2 where $E_z = e_z(r, \phi)e^{-j\beta z}$ and $k_c = k^2 - \beta^2$ should be solved. Solution of this equation is in the form 3-3 where $J_n(k_c r)$ is the Bessel function.

$$(\frac{\partial^2}{\partial r^2} + \frac{1}{r}\frac{\partial}{\partial r} + \frac{1}{r^2}\frac{\partial^2}{\partial \phi^2} + k_c{}^2)e_z = 0 \tag{3-2}$$

$$e_z(r, \phi) = (A sin(n\phi) + B cos(n\phi))J_n(k_c r) \tag{3-3}$$

PEC boundary starts from the radius of the circular waveguide, $r = a$. So, tangential electric field component should be zero on the boundary which impose the $E_z = 0$ when $r = a$. Therefore, equation 3-4 where p_{nm} is the root of Bessel function should be satisfied. Propagation constant of the TM_{nm} mode is given in the equation 3-5 and the cutoff frequency is given 3-6. Roots of the Bessel functions can be found in

22

mathematical tables [3].

$$k_{\mathrm{c}} = \frac{p_{\mathrm{nm}}}{a} \tag{3-4}$$

$$\beta_{\mathrm{mn}} = \sqrt{k^2 - (p_{\mathrm{mn}}/a)^2} \tag{3-5}$$

$$f_{\mathrm{c}_{\mathrm{nm}}} = \frac{k_{\mathrm{c}}}{2\pi\sqrt{\mu\epsilon}} \tag{3-6}$$

If same procedure is applied to TE modes ,cutoff frequencies can be obtained. Lowest order modes of circular waveguides based on above equation are as follows TE_{11}, TM_{01}, TE_{21},TE_{01} and T_{11},TE_{31},TM_{21} ...

3.2 Group Velocity and Phase Velocity

Phase and group velocity are two important concepts to investigate the Cherenkov resonance condition which impose to equalize the electron beam velocity with the phase velocity of the electromagnetic wave. Phase velocity is the speed at which a constant phase point travels. Phase velocity is equal to the speed of light for TEM wave. However, phase velocity can be greater or less than the speed of light for guided wave propagation. Phase velocity can change in some medium with respect to frequency. Such a medium is called as dispersive media and such an effect is called as dispersion effect. Different phase velocities allow faster waves or slower waves. Phase velocity is expressed in Equation 3-7.

$$V_{\mathrm{p}} = \frac{\omega}{k} \tag{3-7}$$

Group velocity is the velocity of the wave energy flowing in the direction of the Poynting vector. This means energy or information can be carried out by group velocity. It is worth to note that if the group velocity is in the opposite direction of the phase

velocity, propagation of the wave is called backward wave.

$$V_{\mathrm{g}} = \frac{\partial \omega}{\partial k} \tag{3-8}$$

3.3 Dispersion Relation

Dispersion occurs when the phase velocity of the wave varies with frequency. Investigating the dispersion are possible with two ways. First, obtaining phase velocity of the medium in different frequencies. Second, Brillouin diagram or $\omega - \beta$ diagram can be obtained. Brillouin diagram represents the relationship between the angular frequency and the propagation constant. If we compare the common transmission lines and waveguides in terms of dispersion relation, we can see that while the waveguide is dispersive, coaxial transmission line is not dispersive. In addition to that stripline is not dispersive and microstripline has small dispersion since it supports quasi TEM. To claim that, TEM waves are nondispersive will be true. Besides, TM and TE waves exhibit dispersion at the same time. Dispersion diagram can represent the stopband and passband region, forward and backward wave propagation and also resonant frequency intervals for SWS. Figure 3.2 represents the dispersion diagram of the SWS used in this thesis.
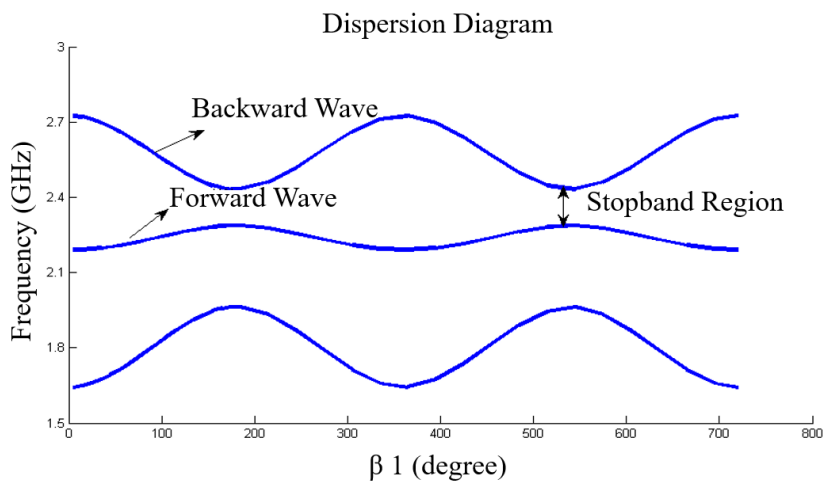
Figure 3.2: Dispersion Diagram of the Lowest Order Modes

24

From the resonance frequencies of the SWS cavity, dispersion diagram can be derived. Synthetic technique to derive dispersion diagram from resonant frequencies was suggested in [75]. Using this technique, dispersion diagram is observed from resonant frequencies in [75]. Relation between resonant frequencies and propagation constant can be expressed as

$$f = \sum_{m=0}^{\infty} a_{\mathrm{m}} cos(m\beta p) \tag{3-9}$$

where β is the angular wavenumber, p is the periodic length of the SWS cell, a_{m} are coefficients. These coefficients can be derived from the measured resonant frequencies using the βp as phase shift per period.

3.4 Interaction Impedance

BWO is based on beam wave interaction principle. To characterize this interaction interaction impedance is defined as in Equation 3-10. This equation is introduced by Pierce in 1950 for the TWT. Increasing the interaction impedance will result in high electronic efficiency. To increase the efficiency, it is important to examine the key parameters that affect interaction impedance. In the absence of the beam, interaction impedance is defined as

$$K_{\mathrm{o}} = \frac{|E_{\mathrm{zm}}|^2}{2\beta_{\mathrm{zm}}^2 W v_{\mathrm{g}}} \tag{3-10}$$

where $E_{\mathrm{zm}}, \beta_{\mathrm{zm}}, W$ and v_{g} represent the axial electric field component, propagation constant of the mth spatial harmonic, energy stored per waveguide period and group velocity respectively. Equation 3-10 implies the interaction impedance can be increased by improving the axial electric field component of the interacting the TM mode. To achieve this, design should provide TM mode dominance in order to increase the axial electric field component. Another way to improve interaction impedance is to reduce the group velocity or decreasing the stored energy per unit cell. High TM mode dominance and low group velocity is the aim of designing SWS.

3.5 Electron Beam

Electron beams are flows of free electrons moving in the direction which is called as beam axis [76]. Electron beam can be generated by thermionic emission, secondary electron emission or field emission. Thermionic emission is the discharge of electrons from heated materials. Emission occurs because the thermal energy given to the charge overcomes the work function of the metal. Current density of the thermal emission is expressed as the Richardson's law [77]. Secondary emission is observed when incident particles with sufficient energy hit the surface or passing through some material. It can occur in the vacuum tube devices when electrons from the cathode strikes the anode. It may cause parasitic oscillation. Field emission is emission of electrons by strong electrostatic fields. This type of emission can be used in electron guns for high power microwave sources. Electrostatic field is generated between anode and cathode of the electron gun with high voltage sources. Maximum current density generated by field emission can be limited by space charge [78]. Electron beam is generated by electron gun in high power microwaves. The design parameters are beam current, perveance, beam radius. In this thesis, electron gun is not designed for electron beam generation. Instead of that generated electron beam is used with electron beam current, energy and beam radius in DC emission model in CST Particle Studio.

3.6 Backward Cherenkov Radiation

In 1934, Cherenkov radiation is discovered experimentally by the Pavel Alekseyevich Cherenkov [79] .Charged particles moving in the medium with a speed slightly greater than the phase velocity of electromagnetic wave in that medium emit Cherenkov radiation. If the emitted radiation and charged particles velocity are in the same direction it is termed as forward Cherenkov radiation. If the electromagnetic wave is generated in the reverse direction of electron beam, this is termed as reversed Cherenkov radiation. It signs the metamaterial media since it provides backward wave propaga-

26

tion. To provide reversed Cherenkov radiation, the below condition must be satisfied.

$$\omega - k_z v_z = 0 \tag{3-11}$$

In Equation 3-11, ω is the angular frequency, v_z is the axial electron velocity and k_z is the axial wave number. There are very few experiments on reversed Cherenkov radiation since to provide double negative media using full metal is challenging. Metallic structure should be used to observe reversed Cherenkov radiation since high voltage causes dielectric breakdown for dielectric structure. Electron beam passing through the MTM produce the reversed Cherenkov radiation in the double negative frequency band in [66]. Reversed Cherenkov radiation is aimed to observe in [64]. However, they indicate that instead of Cherenkov instability, the Cherenkov-cyclotron instability dominates the operation in double negative media.

3.7 Cherenkov-Cyclotron Instabilities

Theoretical analysis of the beam wave interaction for metamaterial is considered in terms of the the possibility of reverse (or backward) Cherenkov radiation [64]. However, they observed the Cherenkov-Cyclotron instabilities dominance. The general expression [81] that describes the Cherenkov-Cyclotron instabilities is given as

$$\omega - k_z v_z = n\Omega_c/\gamma \tag{3-12}$$

where ω is the angular frequency, v_z is the axial electron velocity, k_z is the axial wave number, $n\Omega$ is the cyclotron frequency, γ is the Lorentz factor and n is the resonant harmonic which is equal to -1 for BWO [64]. Cyclotron frequency is the frequency of a charged particle moving perpendicular to the direction of a uniform magnetic field. This motion is always circular, so the cyclotron frequency can be described considering the centripetal force and magnetic Lorentz force.

$$\frac{mv^2}{r} = qBv \tag{3-13}$$

27

$$\omega = \frac{v}{r} = \frac{qB}{m} \tag{3-14}$$

In Equation 3-14, q is the electron charge, B is the magnetic field and m is the electron mass. Lorentz factor represents relativistic mass change for an moving object. Equation 3-15 represents the Lorentz factor.

$$\gamma = \frac{1}{\sqrt{1 - \frac{v_z^2}{c^2}}} \tag{3-15}$$

Instability occurs when the cold dispersion curve and Cherenkov or Cherenkov-Cylotron instability curve intersects. Also, it is worth to note that the electromagnetic fields in metamaterial is difficult in analytical methods so we should trust the numerical methods.

3.8 Introduction to Metamaterial

Metamaterials are artificially created periodic materials with a period generally much smaller than the wavelength. Properties of metamaterial are not observed in the nature. Unique metamaterials properties are negative index refraction, supporting backward wave propagation or opposite sign in phase and group velocities, reversed Cherenkov radiation, inverse Doppler Effect. Metamaterials are also called as left-handed materials since wave vectors $\vec{k}$ is the left handed triplet of the electric field vector $\vec{E}$ and magnetic field vector $\vec{H}$. In 1968, Veselago predicts the negative permittivity and permeability theoretically [60]. Some metamaterials have only one negative permittivity like plasmas or only negative permeability such as magnetized ferrites and some of them can show both negative permittivity and permeability as experimentally validated by Pendry [82].

To begin with, constitutive parameters relation is a good point to better understand the metamaterial properties. For a homogenous medium, the constitutive parameters

are represented as in Equation 3-16 and 3-17.

$$\vec{D} = \epsilon \vec{E} \qquad (3\text{-}16)$$

$$\vec{B} = \mu \vec{H} \qquad (3\text{-}17)$$

However, constitutive parameters are frequency dependent parameters for dispersive media. The Drude-Lorentz model can be used to express the constitutive parameters in dispersive media.

$$\epsilon(\omega) = 1 - \frac{\omega_{\mathrm{p}}^2 - \omega_{0\mathrm{e}}^2}{\omega(\omega + j\Gamma_{\mathrm{e}}) - \omega_{0\mathrm{e}}^2} \qquad (3\text{-}18)$$

$$\mu(\omega) = 1 - \frac{F\omega^2}{\omega(\omega + j\Gamma_{\mathrm{m}}) - \omega_{0\mathrm{m}}^2} \qquad (3\text{-}19)$$

where ω_{p} is the plasma frequency and $\omega_{0\mathrm{e}}$ is the electric resonant frequency and $\omega_{0\mathrm{m}}$ is the magnetic resonant frequency . Γ is the damping factor represents the material loss. F is the filling ratio factor shows the ratio of the volume of the scattering material to total volume. When the ϵ and μ are negative, it forms the left handed medium. Considering the dispersive media constitutive parameters are written as follows:

$$\vec{D} = \epsilon(\omega) \vec{E} \qquad (3\text{-}20)$$

$$\vec{B} = \mu(\omega) \vec{H} \qquad (3\text{-}21)$$

Refractive index represented by n shows the speed of electromagnetic waves with respect to the light speed. From the Equations 3-22, to obseerve the negative refractive index, $n < 0$, may not be clear because of the square root term. It has been shown in [82]. To understand the negative refractive index boundary conditions are crucial.

Figure 3.3 shows the negative refraction of incident wave. It is possible when the refractive indices of two materials are in opposite signs.

$$n(\omega) = \sqrt{\epsilon(\omega)\mu(\omega)} \qquad (3\text{-}22)$$
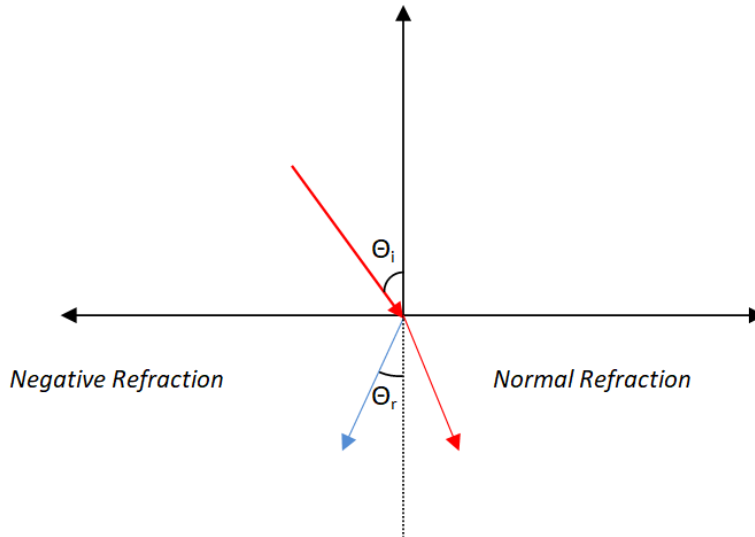
Figure 3.3: Snell's Law in the negative refraction index

Besides that, double negative materials must be dispersive always. The energy density of a dispersive medium is written as in Equation 3-23. Assuming the medium is not dispersive, energy density is negative which is not valid. This proves that double negative medium is always dispersive.

$$W = \frac{\partial(\omega\epsilon)}{\partial\omega}E^2 + \frac{\partial(\omega\mu)}{\partial\omega}H^2 \qquad (3\text{-}23)$$

To define the ϵ and μ for metamaterial is complicated process since they are inhomogeneous periodic structures. Average effect of the unit cell is considered in order to define the permittivity and permeability of unit cell. Different methods to define the constitutive parameters of the unit cell are reported. Generally, scattering parameters are used to extract the constitutive parameters. Since the analytically calculate MTM

is difficult process, numerical methods is used with full wave solver such as CST Studio Suite. In [85], S parameters are used to extract constitutive parameters. However, this method suffers from determining the unique solution. Better solution in [86] is suggested to extract the effective constitutive parameters. They used Kramers-Kronig relations to find unique solution. However, this method has also some limitation to find unique solution and uncertainty.

CHAPTER 4

DESIGN AND SIMULATION OF SLOW WAVE STRUCTURE

4.1 Simulation Environment : CST Studio Suite

In this thesis, simulations are carried using Computer Simulation Technologies (CST) software. CST Studio Suite is software which enables to make 3D EM analysis for design, analyzing and optimizing EM components and systems. CST Studio Suite is an integrated tool for different applications such as antenna and filter design, electromagnetic compatibility and interference, exposure of the human body to fields, electro-mechanical effects in motors and generators and thermal effects in high-power devices [73]. For these applications, different types of solvers are required. In this thesis, Time domain, Frequency domain, Eigen Mode and Particle-in-cell solver will be used.

4.1.1 Time Domain Solver

Time domain solver calculates the development of fields at discrete times and locations. It can calculate the energy flow from one port to another port. Since it calculates fields through time, it is possible to obtain entire broadband frequency behavior in a single run. In CST, two time domain solvers are available that are transient solver and transmission line solver (TLM) solver. Transient solver is based on Finite Integration Technique (FIT) and TLM is based on transmission line method.

The main aspects of the FIT are explained to give insight to Time Domain Solver. FIT discretizes the integral form of Maxwell's equations in Equations 4-1-4-4 to solve these. To discretize the calculation domain CST uses mesh cell as shown in Figure

4.1. Considering Faraday's Law, closed integral in equation 4-1 can be written as the sum of the four voltages in mesh cell which are e_k, e_l, e_m, e_n as shown in Figure 4.1.

$$\int_{\partial A} \vec{E} \cdot d\vec{s} = \int_{A} \frac{\partial \vec{B}}{\partial t} \cdot d\vec{A} \qquad (4\text{-}1)$$

$$\int_{\partial A} \vec{H} \cdot d\vec{s} = \int_{A} (\frac{\partial \vec{D}}{\partial t} + \vec{J}) \cdot d\vec{A} \qquad (4\text{-}2)$$

$$\int_{\partial V} \vec{D} \cdot d\vec{A} = \int_{V} \rho dV \qquad (4\text{-}3)$$

$$\int_{\partial V} \vec{B} \cdot d\vec{A} = 0 \qquad (4\text{-}4)$$
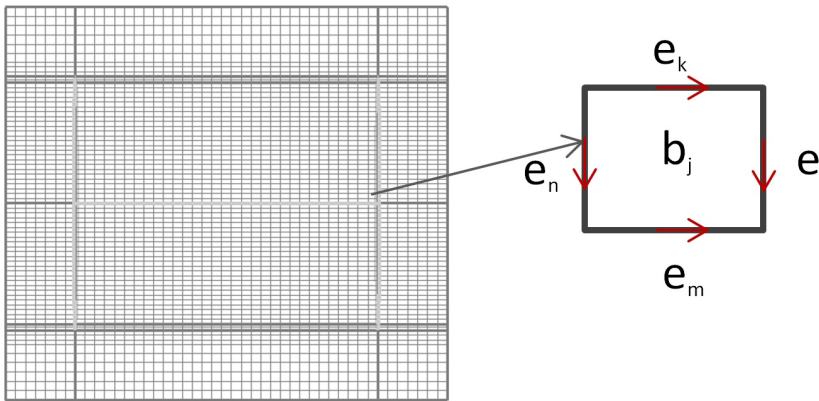
Figure 4.1: Mesh Cells in CST

Time derivative of magnetic flux represented by b_j in Figure 4.1 can be written as the right hand side of the equation 4-1. Repeating the this procedure to all available mesh cell creates the matrix formulation introducing the topological matrix **C** as in the equation 4-5 and equation 4-6. Four equations are converted to matrix form as in Ampere's Law. In addition to that constitutive relations are added. At the end, all matrix equations are available to solve electromagnetic field problems on the discrete

grid space.

$$e_k + e_l - e_m - e_n = -\frac{\partial b_j}{\partial t} \tag{4-5}$$

$$\underbrace{\begin{pmatrix} \cdots & \cdots \\ 1 & 1 & -1 & -1 \\ \cdots & \cdots \end{pmatrix}}_{C} \underbrace{\begin{pmatrix} e_k \\ e_l \\ e_m \\ e_n \end{pmatrix}}_{e} = -\frac{\partial}{\partial t} \underbrace{\begin{pmatrix} \cdot \\ b_j \\ \cdot \end{pmatrix}}_{b} \tag{4-6}$$

4.1.2   Frequency Domain Solver

Frequency domain solver has to carry out the simulation for a frequency. Every frequency sample requires solving an equation system. As distinct from time domain solver, Maxwell's equations is transformed to frequency domain and the fields are represented by phasors. In frequency domain solver, it is not possible to observe the entire broadband frequency behavior in a single run as in time domain solver because it carries out the calculation frequency by frequency. Key applications of frequency domain are strongly resonance structures.

4.1.3   Eigen Mode Solver

Eigen mode solver calculates the frequencies and the corresponding electromagnetic field patterns without excitation. Results of eigen mode solver are the field distribution of the modes and the eigenfrequencies of the structures. The eigenmodes and their frequencies are the solutions of the eigenvalue equation 4-7. There are two solvers available: the Advanced Krylov Subspace method (AKS) and the Jacobi-Davidson method (JDM). The AKS solver calculates the a number of modes with lowest resonant frequencies in loss free structures. The JDM solver can include losses

in calculation.

$$\nabla x \nabla x \mathrm{E} = -\mu\epsilon\frac{\partial^2 \mathrm{E}}{\partial t^2} \qquad (4\text{-}7)$$

4.1.4 Particle-in-cell Solver

The Particle In Cell (PIC) solver is used to calculate fields and particles through time at discrete time samples. Fields calculation is like in time domain solver whereas particles are tracked in continuous phase space. Interaction between electron motion and fields is calculated iteratively shown in Figure 4.2.
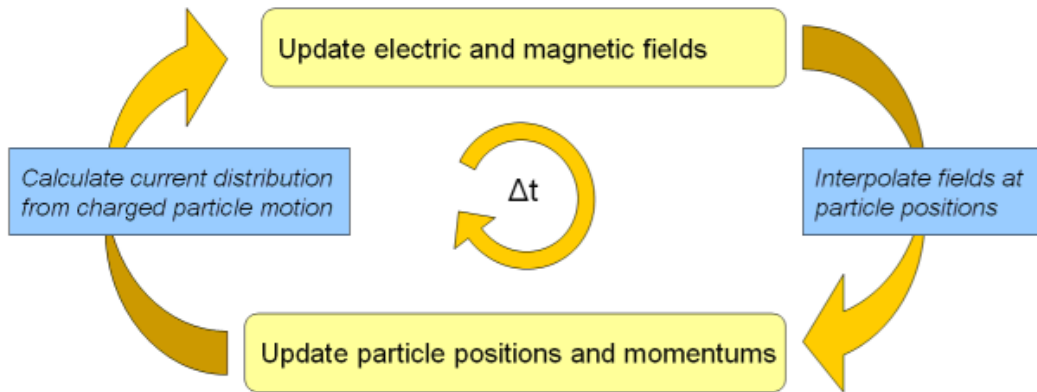
Figure 4.2: PIC Solver Interpolation Schemes

There are different emission models in PIC solver which are gauss , DC and explosive emission. These are used to emit particles. In DC emission models, emission current is fixed. Kinetic energy of beam should be adjusted by user. The Gauss emission model describes a pulsed particle emission. Voltage should be applied to generate electric field in explosive emission models. Beam is generated by electric field close to the cathode. In this thesis, DC emission model is used for BWO simulation.

4.2 Cold Test Simulation of SWS

As explained in previous sections, metamaterials are periodic structures which supports reversed Cherenkov radiation since it provides negative refractive index. Be-

sides that, MTM loaded waveguide decreases the phase velocity of electromagnetic wave comparing with hollow waveguide which is required to provide synchronism condition. Considering all of these, MTMs are attractive candidates for slow wave structure of high power microwaves.

Here, the goal is the design novel metamaterial based rectangular slow wave structure for high-power microwave source BWO. Metamaterial based rectangular slow wave structure as in Figure 4.3 is observed for the different modes. To achieve that, phase velocity of electromagnetic wave is slowed to the speed of electrons to provide synchronism condition. Besides that, one of the design goals is miniaturization of the SWS using the metamaterial unique properties which is the evanescent mode propagation. Using the metamaterial shown in Figure 4.3 wave propagation is provided for the frequencies that are below the cutoff frequency of the hollow waveguide. To investigate the electron beam coupling to metamaterial slow wave structure, interaction impedance should be high as much as possible. To increase the interaction impedance of the SWS is the one of the design goals. Interaction impedance of the proposed SWS is also observed. Since the dielectrics suffer from dielectric breakdown for high power microwaves, full metal slow wave structure design is also aimed. To begin with, the unit cell configuration in Figure 4.3 and Table 4.1 show the dimensions of the slow wave structure. Rectangular SWS are connected to waveguide using 30°tab.

SWS is analyzed using the dispersion relation. Dispersion diagram of the desired mode adjusted to operation frequency interval which is aimed as 2.4-2.5 GHz. In order to analyze the dispersion relation of the unit cell, CST Studio Suite was used with Eigen Mode Solver. Unit cell of the SWS is shown in Figure 4.4 . While X and Y directions are PEC boundary, this unit cell is periodic in the Z direction as Eigen Mode Solver dictates. Eigen Mode Solver gives phase shift in the axial direction of the unit cell. Then, it repeats the different phase shifts to find dispersion relation of the unit cell. The dispersion diagram represents frequency and wave number relation for different modes. Dispersion diagram is simulated without electron beam which is the reason the simulation is termed as cold test simulation. Dispersion diagram for 8 lowest order modes of the rectangular SWS is shown in Figure 4.5. To define the modes in SWS is difficult because of the complexity of the geometry.
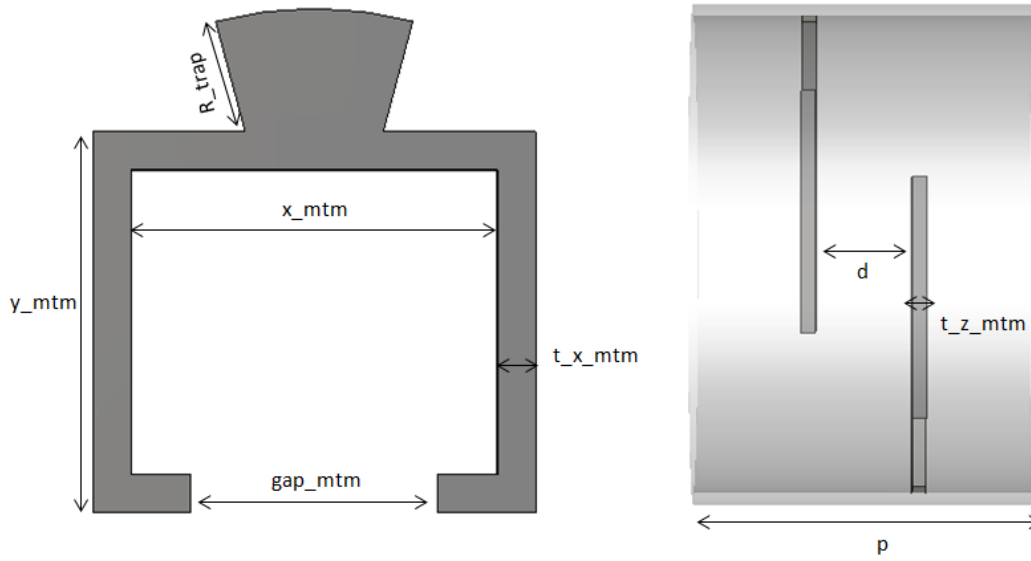
Figure 4.3: Geometry of the SWS

(a)   (b)
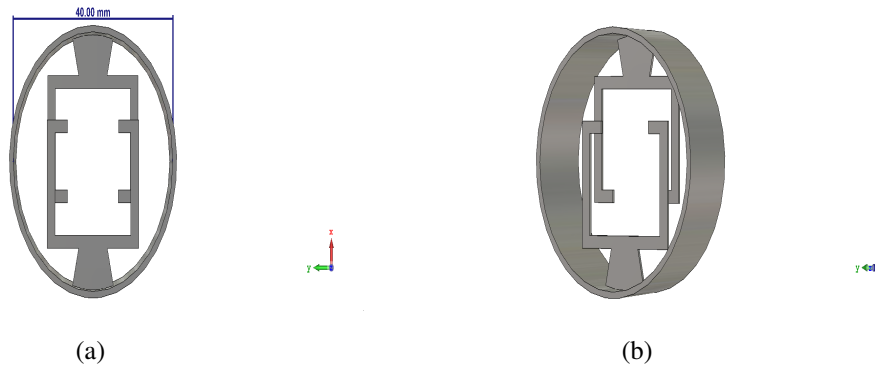
Figure 4.4: (a) Dimension of the SWS (b) One unit of the SWS

Table 4.1: Dimension of SWS.

Parameter Name	x_mtm	y_mtm	gap_mtm	t_x_mtm	R_trap	p	d	t_z_mtm
Unit:mm	19.25	20.00	13.00	2.00	6.00	25.00	7.00	1.00

38

So, modes are called with numbers such as mode 1, mode 2 and their properties such as TM-like mode and TE-like mode in thesis. Although first two modes of the hollow cylindrical waveguide are degenerate modes on simulation as in Figure 4.7, this is not the case for SWS since added metamaterial disturbs the symmetry.
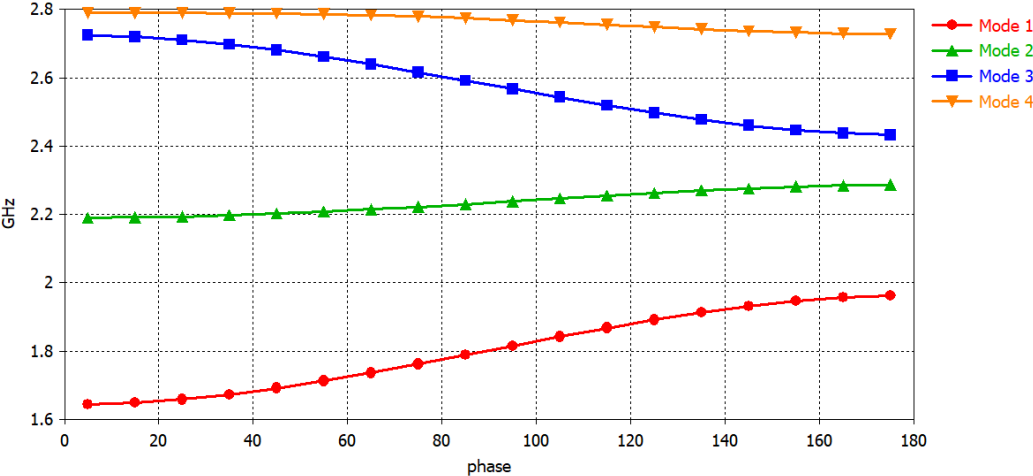
(a)
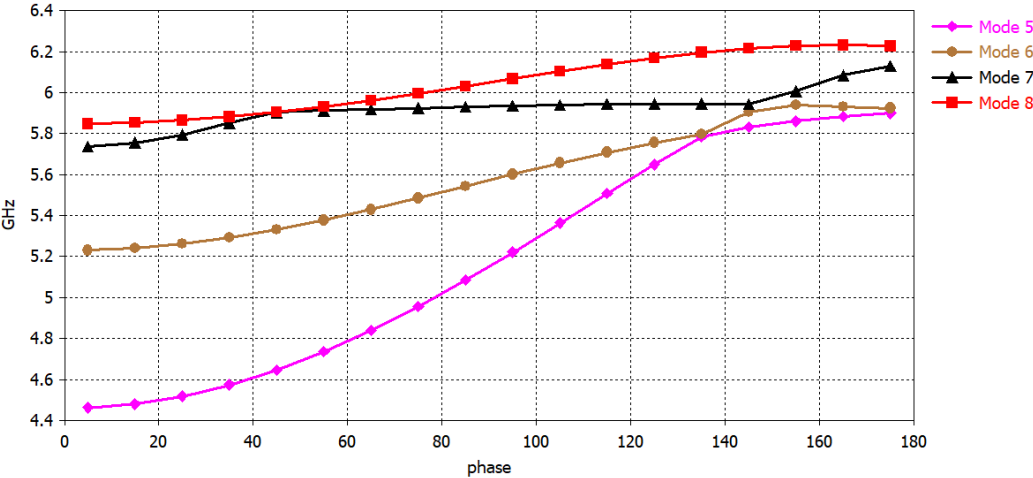
(b)

Figure 4.5: (a) Dispersion diagram of lowest order first 4 modes (b) Dispersion diagram of lowest order second 4 modes

According to theory of BWO [48] , the operation mode is the TM mode. In addition to that double negative media supports TM mode propagation below cutoff frequency. These two shows that operation mode is TM mode. However, reflections

from electron gun can excite undesired modes. Also, TM_{01} is not the fundamental mode for circular waveguide. This results in hybrid mode excitation in SWS. Following sections are dedicated to investigate modes on hollow circular waveguide and SWS loaded circular waveguide.

4.2.1   Mode Analysis of Circular Waveguide

Hollow circular waveguide can support TE and TM modes. Theoretical subjects about hollow circular waveguide processed in the section 3. In this part, simulation based investigation of hollow circular waveguide will be the subject. Initially, cut-off frequencies of modes are calculated for the hollow waveguide shown in Table 4.2. Electric field of corresponding modes are also shown in Figure 4.6. It is worth the note that, lowest order two modes share the same resonant frequency. These are called as degenerate modes. The reason behind that is based on the symmetry of the hollow circular waveguide. Electric fields of these modes are 90°shifted version of each other as shown in Figure 4.6a and 4.6b. In other words, one of the modes will be degenerated depending on the excitation probe position. So, second order mode is considered as mode in Figure 4.6c which is called as TM_{01}.Lowest order modes of circular waveguides are as follows TE_{11}, TM_{01}, TE_{21},TE_{01} and T_{11},TE_{31},TM_{21} ...

Interaction between electron beam that is guided with strong magnetic field with electromagnetic wave occurs with TM modes due to their strong longitudinal electric field component. So, the operation mode for the hollow circular waveguide will be the TM_{01} which corresponds to **Mode 3** in dispersion diagram Figure 4.5 due to the degenerate modes. Dispersion diagram of the hollow circular waveguide is shown in Figure 4.7. Two degenerate modes are also seen in this plot.

Table 4.2: Cutoff frequencies of circular waveguide with 40 mm diameter.

Mode	Cut-off Frequencies
TE_{11}	4.40 GHz
TM_{01}	5.75 GHz
TE_{01}	7.29 GHz

(a) Fundamental Mode

(b) Degenerate Mode

(c) Second Mode

(d) Third Mode
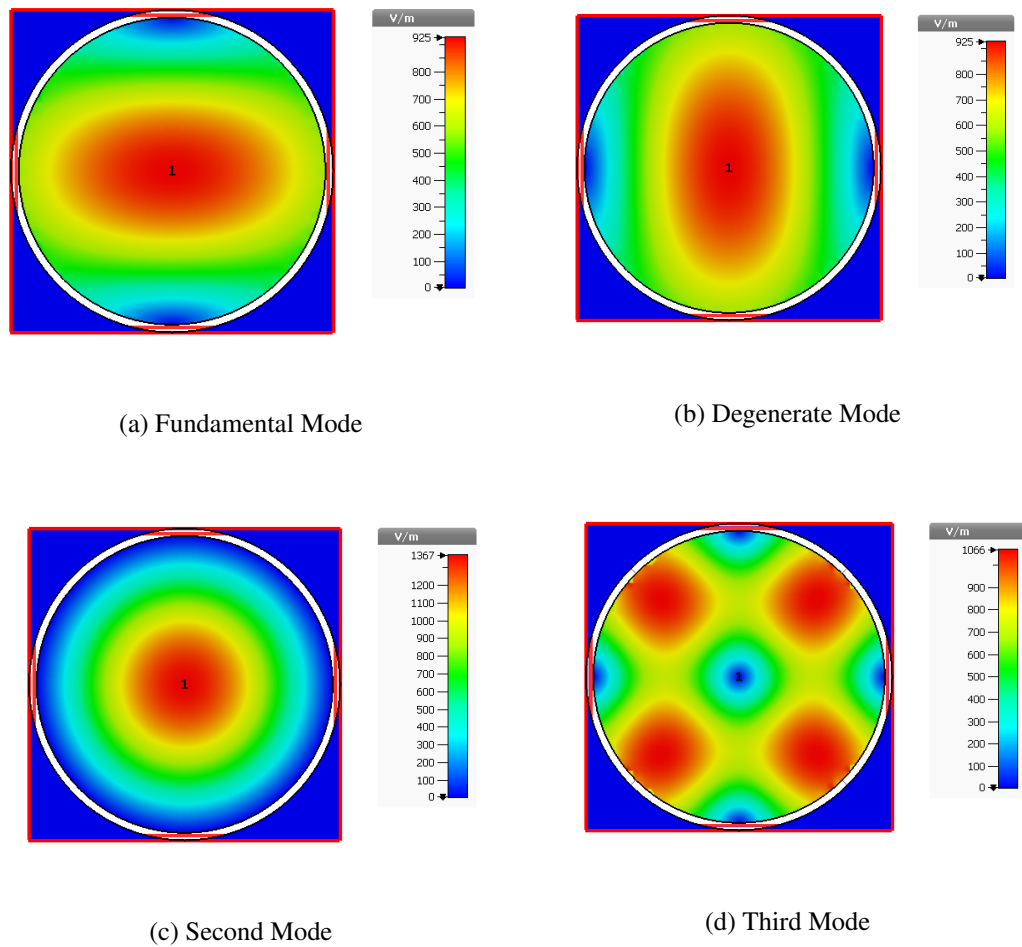
Figure 4.6: Electric Field of Hollow Circular Waveguide for Lowest-order 4 Modes

4.2.2 Analysis of Rectangular SWS Loaded Circular Waveguide

In the previous section, two degenerate modes are illustrated for circular waveguide. This case is changed when we loaded circular waveguide with rectangular SWS as shown in Figure 4.4. These two degenerate modes are not degenerate modes so far. Evidence of this assertion can be shown in dispersion diagram of loaded circular waveguide as in Figure 4.5. There are no overlapping modes in dispersion diagram as in the case of hollow circular waveguide. Also, to compare the magnitude of the axial electric field component E_z and absolute electric field magnitude along the propagation axis can give insight to understand modes. Figure 4.8 to Figure 4.11 show the axial electric field component E_z and absolute electric field magnitude. Mode 1

41
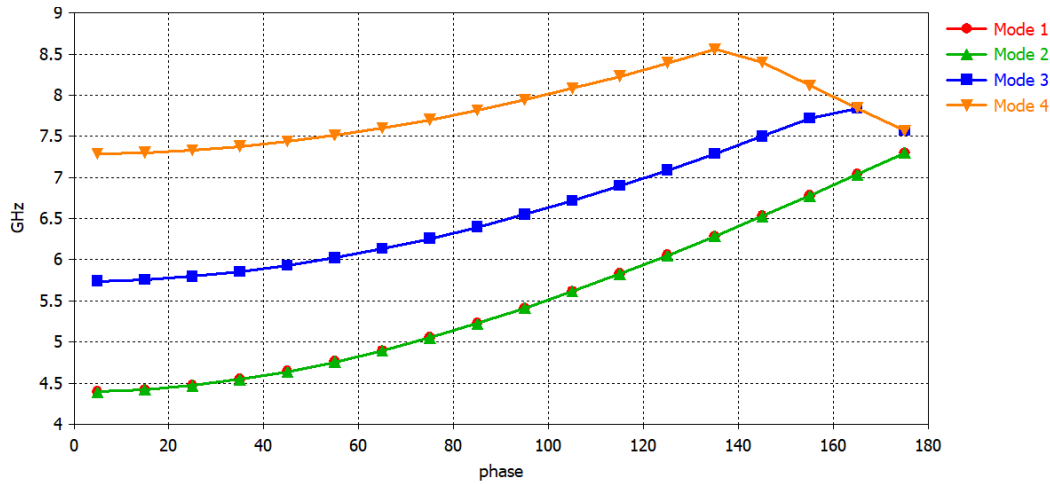
Figure 4.7: Dispersion Diagram of Hollow Circular Waveguide

and Mode 3 are convenient modes to support TM modes.

In order to observe the effect of rectangular slow wave structure, hollow circular waveguide is also simulated in the CST Eigen Mode Solver. Both absolute and axial electric field component are observed. Circular waveguide is used without rectangular slow wave structure component shown in Figure 4.3 . As expected, transverse magnetic field mode operation includes the electric field in the direction of wave propagation. Besides, transverse electric field mode operation does not include the axial electric field component which is in the propagation direction. Below figures shows the axial and absolute electric field of the empty circular waveguide. Since the axial and absolute electric field overlaps, two figures are used to show electric field of the TM_{01}.

In this design, beam-wave interaction occurs with TM-like mode. The wave grows due to the synchronism between the phase velocity of wave and the electron beam velocity. Oscillation frequency of the BWO can be predicted in cold test simulation investigating the frequency where the intersection occurs between phase velocity of operation mode and electron velocity. Dispersion diagram with light line is shown in Figure 4.15. Since the electron velocity will be smaller than the light velocity, oscillation frequency will be lower than the intersection of the dispersion diagram of the light line and Mode 3.

After the TM-like modes and intersection of the dispersion diagram with light line are
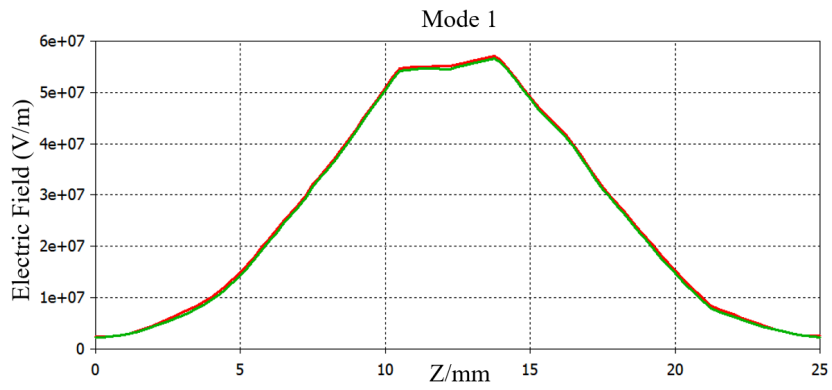
Figure 4.8: Mode 1 Absolute and Axial Component of the Electric Field
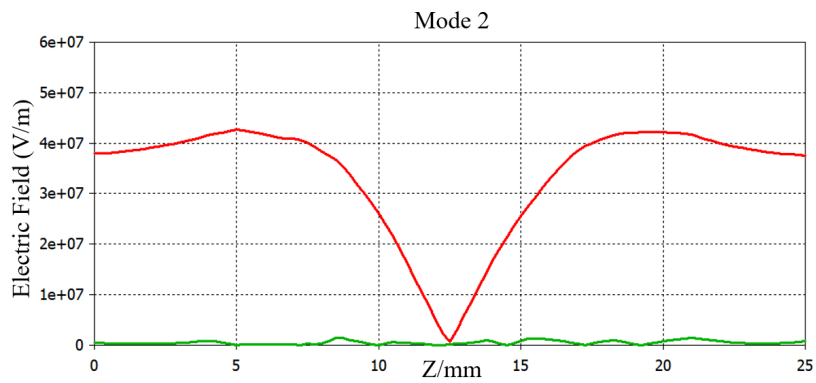
Figure 4.9: Mode 2 Absolute and Axial Component of the Electric Field
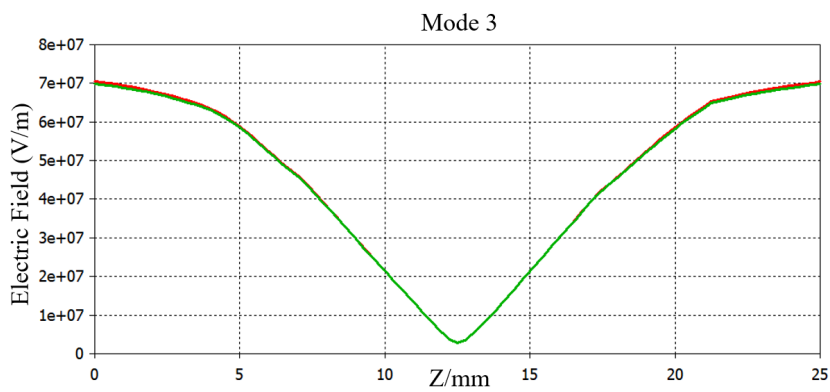
Figure 4.10: Mode 3 Absolute and Axial Component of the Electric Field
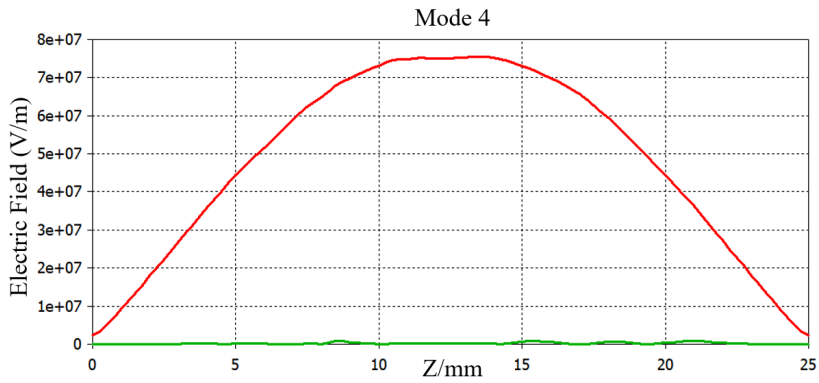
Figure 4.11: Mode 4 Absolute and Axial Component of the Electric Field
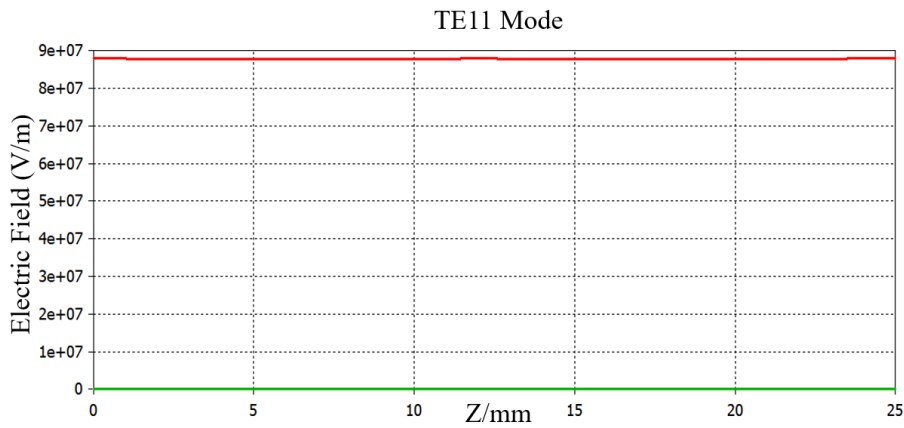
Figure 4.12: TE$_{11}$ Absolute and Axial Component of the Electric Field

observed, next step is to observe phase velocity of the wave. In order to show the SWS slows the phase velocity of the wave, phase velocity of the Mode 3 is plotted using Eigen Mode Solver and equation in 4-8 in Figure 4.16. We investigated the mode 3 since it provides backward waves according to dispersion diagram. Normalized phase velocity of the wave with respect to speed of light is shown here because to prove the structure can provide slow wave. It is known that electromagnetic wave in waveguide has greater phase velocity than light on the contrary of slow wave structure loaded

44
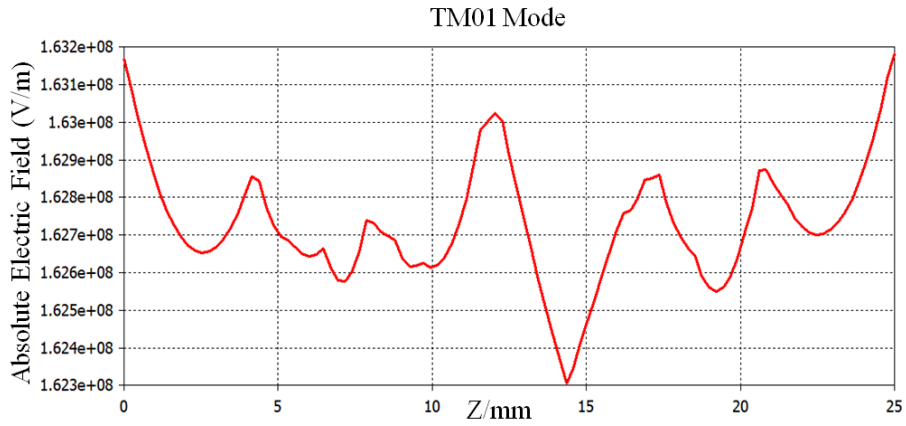
Figure 4.13: TM_{01} Absolute Electric Field
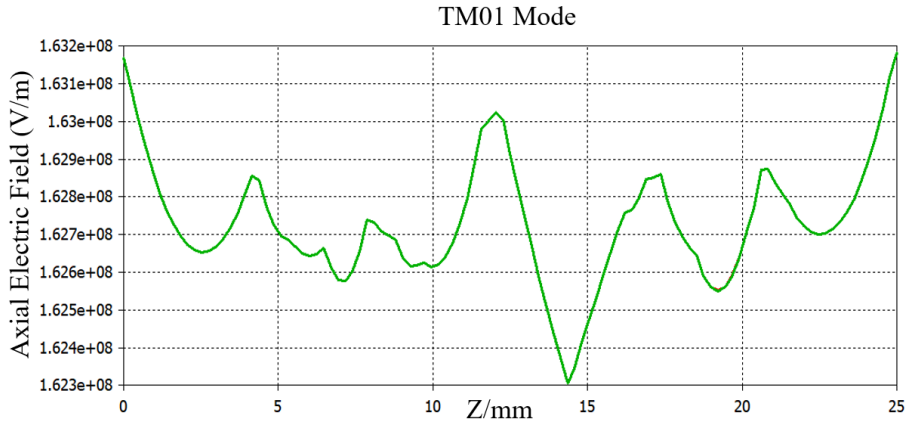
Figure 4.14: TM_{01} Axial Electric Field

waveguide.

$$V_{\mathrm{p}} = \frac{2 \cdot \pi \cdot f}{\beta} \tag{4-8}$$

Providing the negative group velocity is one of the properties of the SWS. The group velocity is the velocity of wave energy flowing in the direction of the Poynthing vector. When the group velocity and phase velocity are in opposite direction, this case is termed as backward wave propagation. Group velocity can be considered as the gradient of the dispersion curve according to equation 4-9 . Group velocity of the

45
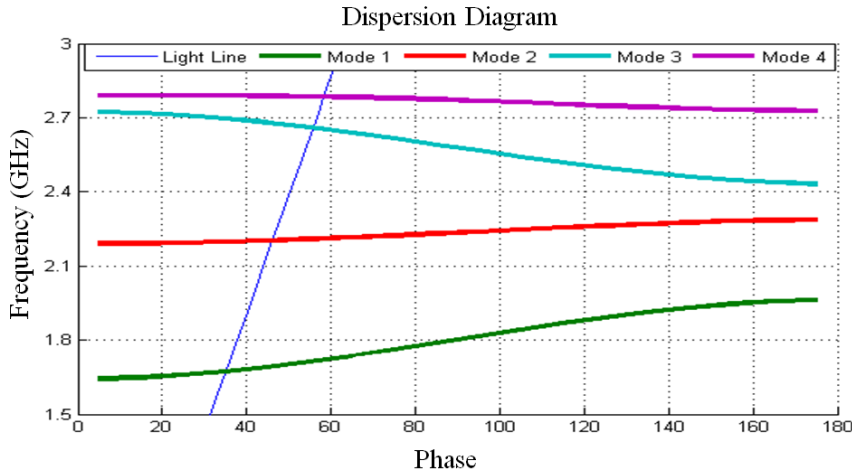
Figure 4.15: Dispersion Diagram of SWS with Light Line
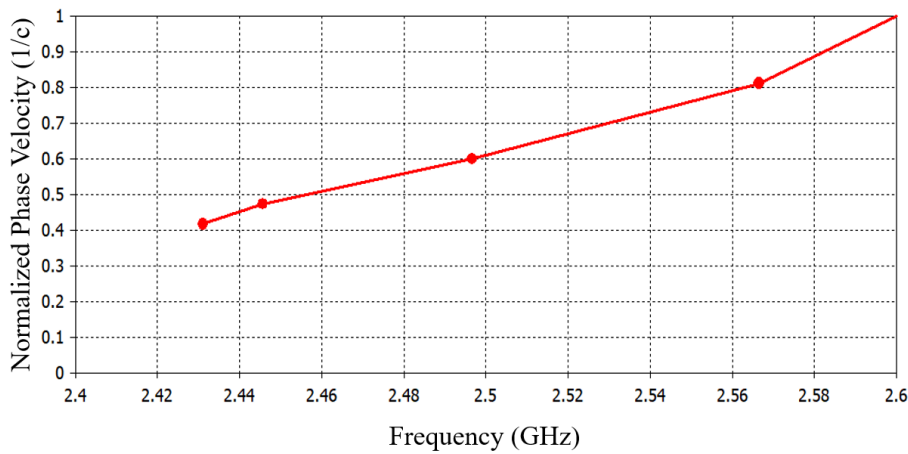
Figure 4.16: Normalized Phase Velocity of the Mode 3

wave in the SWS is observed as in the Figure 4.17. Negative group velocity proves that this structure is appropriate for backward wave propagation.

Interaction impedance is key parameter for efficiency of BWO. As noted, to improve the efficiency is possible with to increase the interaction impedance. To increase the interaction impedance, it is important to examine the parameters that affects the interaction impedance. For TM $_{01}$ mode, interaction impedance can be defined as in the equation 4-10 . To increase the axial electric field component magnitude and

46

decrease the group velocity are the goals of the design. The interaction impedance of the SWS designed in this thesis is shown in Figure 4.18.

$$V_{\mathrm{g}} = 2 \cdot \pi \cdot \frac{\partial f}{\partial \beta} \qquad (4\text{-}9)$$
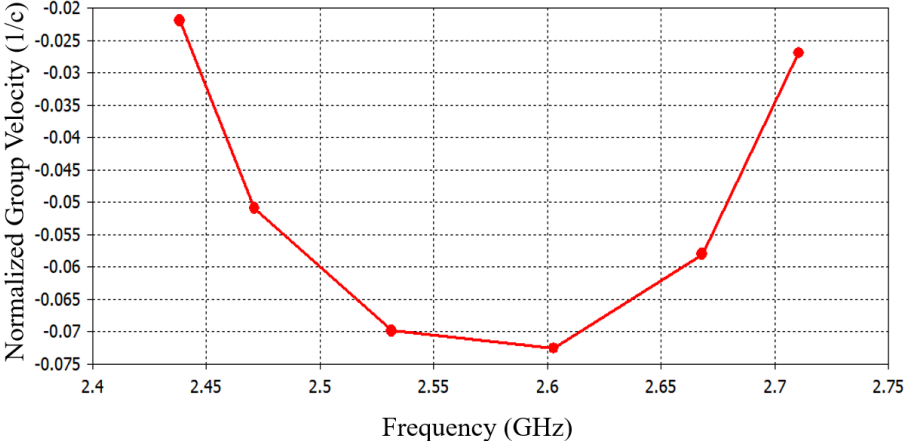
Figure 4.17: Normalized Group Velocity of the Mode 3
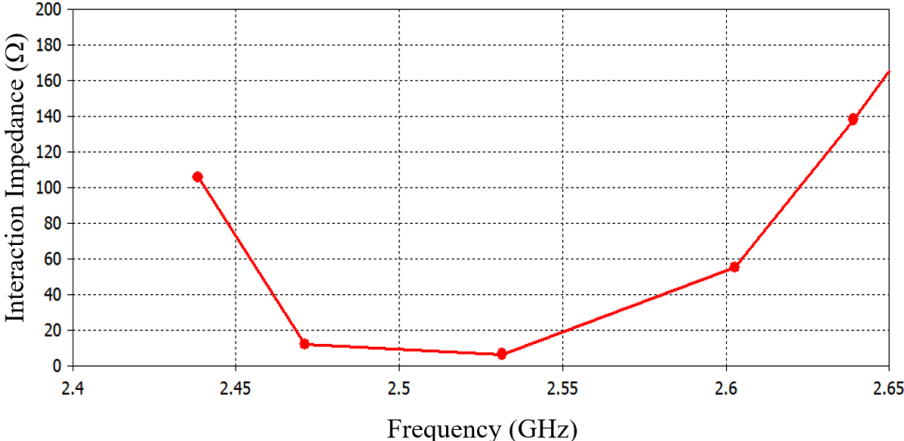
Figure 4.18: Interaction Impedance of the SWS

$$K_{\mathrm{o}} = \frac{|E_{\mathrm{zm}}|^2}{2\beta_{\mathrm{zm}}{}^2 W V_{\mathrm{g}}} \qquad (4\text{-}10)$$

47

4.3 Validation of SWS

In order to synchronize the phase velocity of the wave with speed of electron, to know the dispersion characteristic of slow wave structure is crucial. Analytic method is not appropriate for slow wave structure because of its complexity. Numerical method is used to analyze the dispersion diagram of the slow wave structure. Numerical approach can be applied using Eigen Mode Solver of the commercial 3D electromagnetic solver CST Microwave Studio. Another method is to apply cold test in order to investigate the dispersion characteristics of the SWS and also final verification of the slow wave structure. This process is called cold test since it does not involve the electron beam otherwise it is called as hot test. The cold test is based on that any periodic slow wave structure composed of N unit cell exhibits the N resonance in the 0-π phase interval [90]. To excite the mode properly is crucial for metamaterial SWS. If the modes can not be excited properly, resonant frequencies of SWS cannot be detected [89]. Two important issues should be considered to excite the proper mode which is TM_{01} for our case. First of all, mode launcher should provide sufficient coupling to SWS. Secondly, mode launcher should not excite the different modes. In other words, it should provide the mode purity. There are different types of mode launcher for TM mode excitation in SWS such as cage antenna radiator, rod-wheel radiator, axial loop or axial pin. Before that, TM mode propagation is excited on the hollow circular waveguide with waveguide port. Electric field is observed for the hollow circular waveguide with same radius of SWS as in Figure 4.19.

Mode launcher is simulated in order to validate the TM mode propagation in empty circular waveguide. Simulation is done in Time Domain Solver to analyze broadband frequencies. Hollow circular waveguide is excited by TM mode which is Mode 3. Electric field figure proves that axial pin is appropriate to excite the TM mode as in Figure 4.20. It is worth the note that it can be improved using another type of the mode launcher.

Operation of BWO depends on the TM mode propagation and negative index property of the SWS. So, validation of TM mode propagation in SWS is necessary to use SWS in BWO. We demonstrated the TM mode excitation of empty circular waveguide. When we loaded SWS in waveguide, it supports evanescent mode propagation.

48
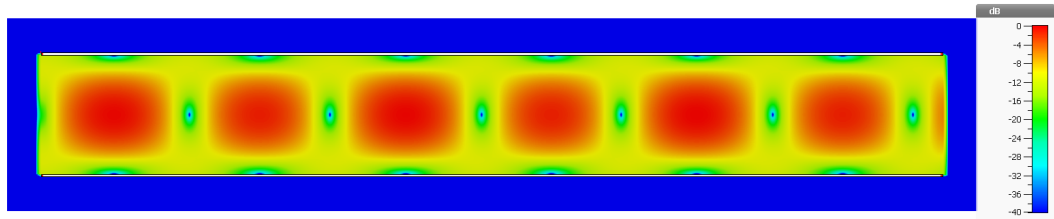
(a) Sectional View on Y Axis
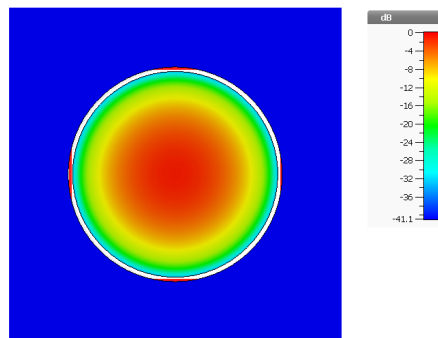
(b) Sectional View on Z Axis

Figure 4.19: Electric Field on the Circular Waveguide for TM_{01}

Designing mode launcher for evanescent mode is impossible in empty waveguide. Therefore, we designed mode launcher in empty waveguide for TM mode. Then, 8 unit cells of the SWS are combined. Complete SWS composed of 8 unit cell shown in Figure 4.21 is simulated with axial pin mode launcher. Mode launcher is designed using parametric analysis. Axial pin length and back short distance are swept and 9 resonances are observed with correlation in dispersion diagram of Mode 3. As emphasized above, N unit cell may exhibit N+1 resonance as shown in Figure 4.27. In addition to that, TM mode propagation is expected for Mode 1 as in Figure 4.8. Resonance also occurs in this mode frequency as in 4.28.
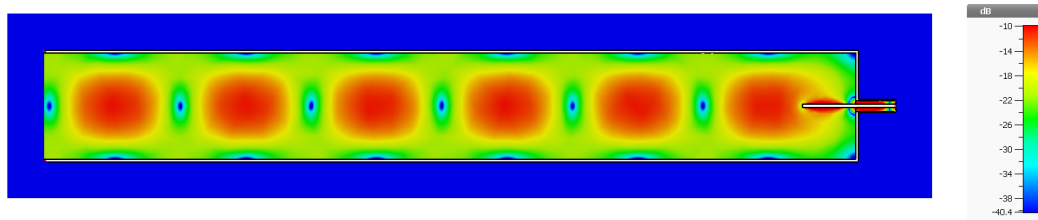
(a)
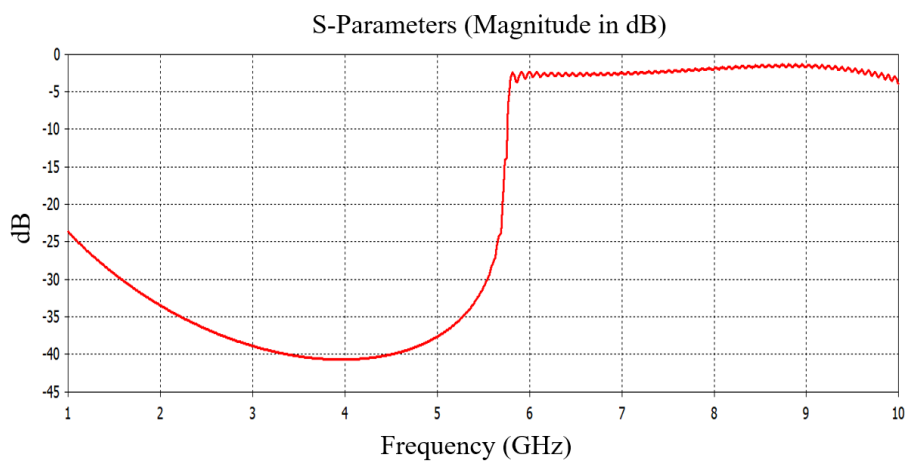
(b)

Figure 4.20: (a) Electric Field of Empty Waveguide Excited by Axial Pin (b) Mode Transmission S2(3)1(1)

Figure 4.29 shows the resonance frequencies for mode 3 and mode 1 frequencies in dispersion diagram. It has strong correlations with the idea that designed MTM structure is suitable for TM mode propagation. Figure 4.8 - 4.11 show that the axial electric field is strongest component for mode 1 and mode 3 which signs the TM mode. Axial electric field component has the biggest contribution to electric field in TM mode propagation.

In order to validate the SWS, the geometry given with Figure 4.22 is fabricated. Fabricated SWS is composed of 3 parts which are shown in Figure 4.23. Part of the

50
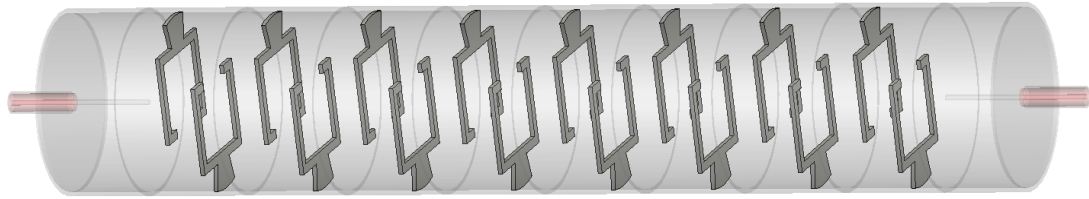
Figure 4.21: 3D Model of SWS Composed of 8 Unit Cell
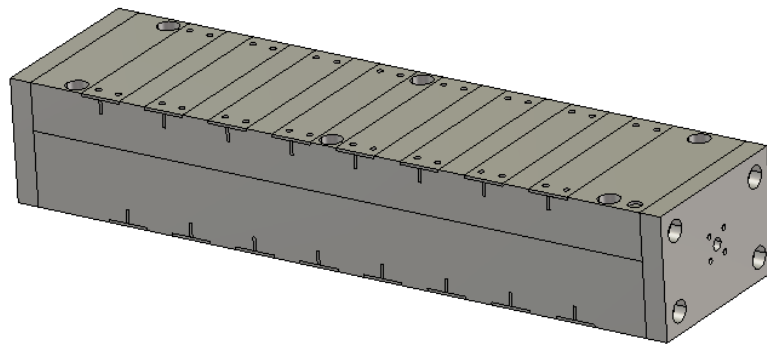
Figure 4.22: 3D Drawing of Fabricated SWS

fabricated SWS shown in Figure 4.23b is fabricated using the laser cutting. Other part shown in Figure 4.23a is fabricated in the CNC machine. Handmade connector shown in 4.24 is used to excite the SWS shown in Figure 4.25. Figure 4.26 shows the axial dimension of the fabricated SWS. Height of the teflon of the handmade connector is 8 mm. The needle is affixed to connector using silver epoxy and adjusted to 19 mm height from teflon.

(a)   (b)
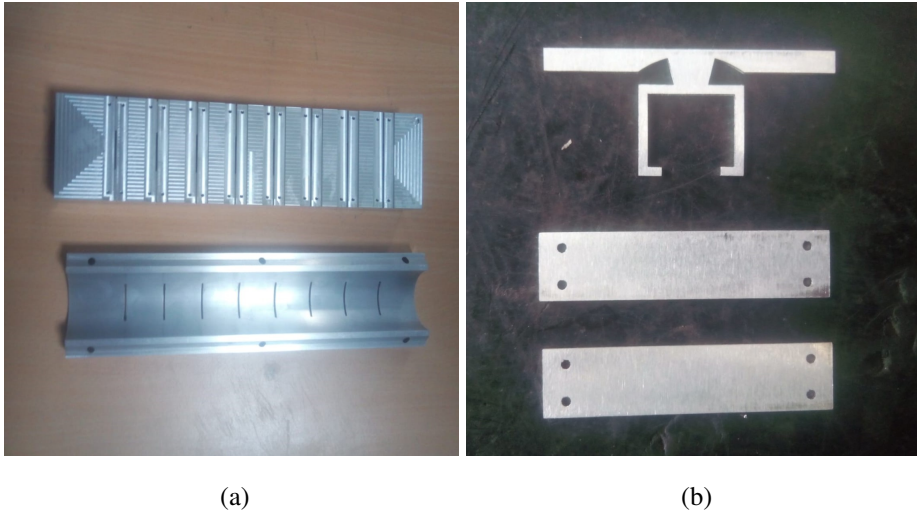
Figure 4.23: Part of the Fabricated SWS

Figure 4.24: Connector of the SWS

TM mode propagation in metamaterial slow wave structure is succeeded using the axial excitation pin shown in 4.24. We observed resonant frequencies in the expected frequency interval which is correlated with mode 1 and mode 3 dispersion diagram. Since to define the modes clearly is not easy, they are called as mode 1 and mode 3. Measurement and simulation results are compared below figures. First two figures show the wideband simulation and measurement of the fabricated SWS. Weak resonance of mode 1 is shown in these figures. Figure 4.32 and 4.33 show the narrowband simulation of the SWS in frequency domain and measurement of the fabricated SWS.

Simulation and measurement results are close to each other. Resonance of the mode 3 is observed.
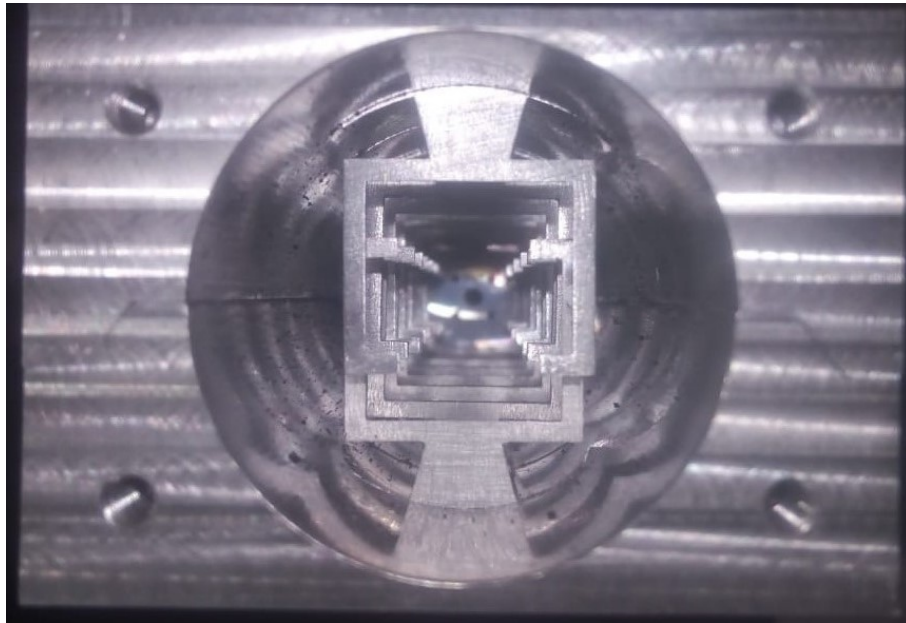
Figure 4.25: Fabricated SWS
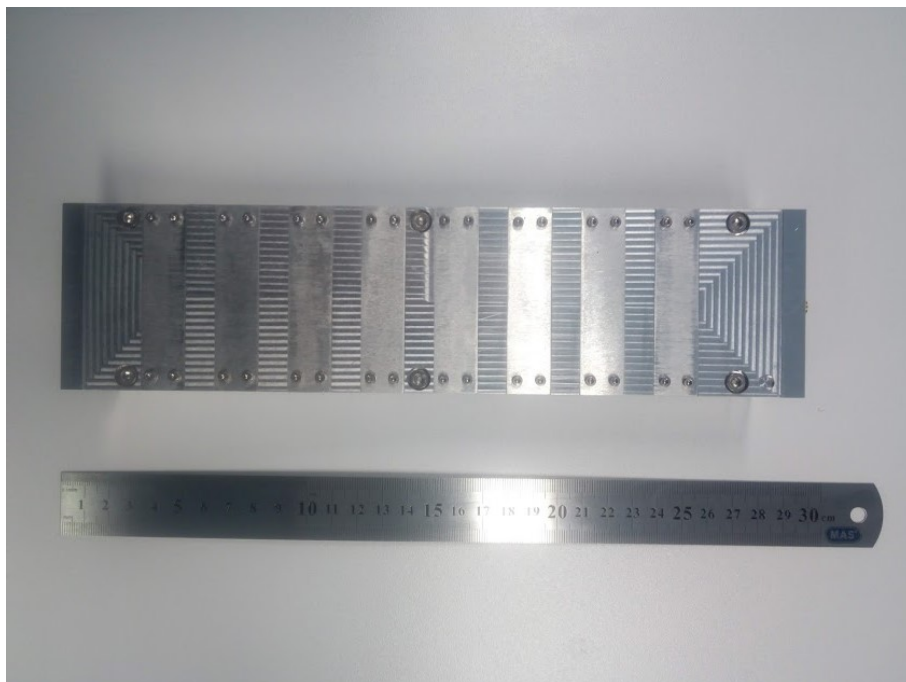
Figure 4.26: Fabricated SWS Dimension
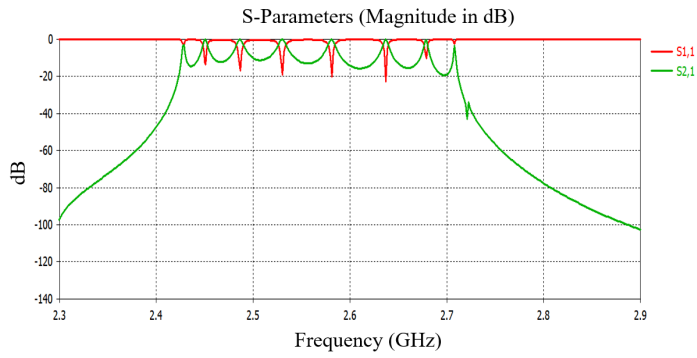
Figure 4.27: S Parameter Simulation of SWS for Mode 3 Frequencies
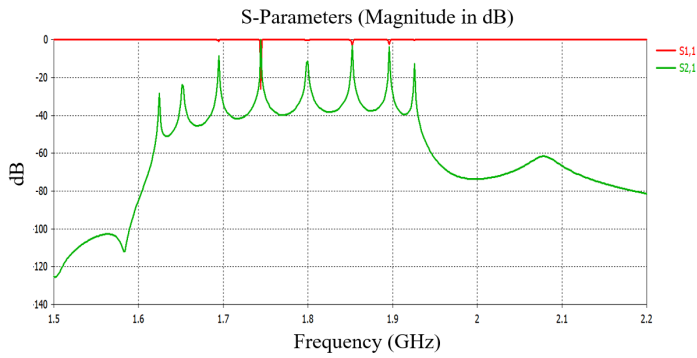
Figure 4.28: S Parameter Simulation of SWS for Mode 1 Frequencies
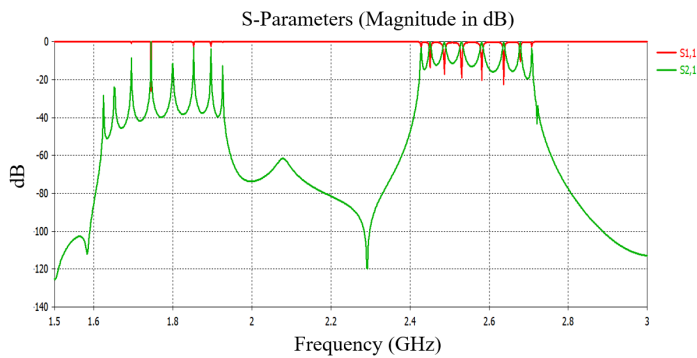
Figure 4.29: S Parameter Simulation of SWS for Mode 1 and Mode 3 Frequencies
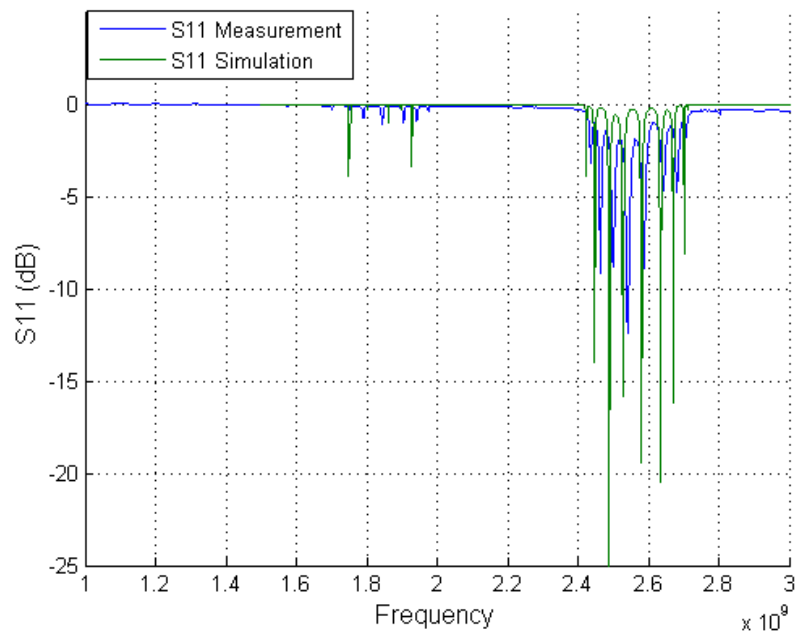
Figure 4.30: S11 of the Fabricated SWS
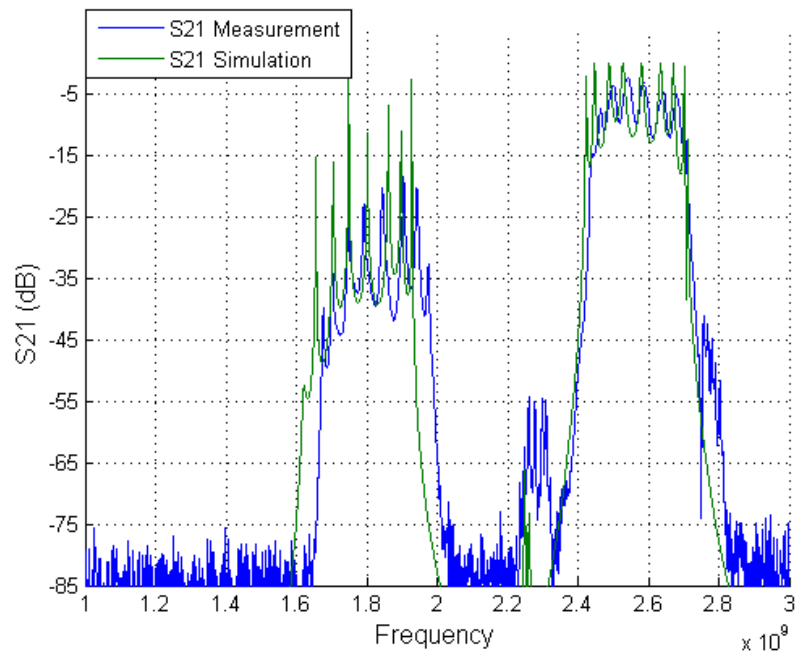
Figure 4.31: S21 of the Fabricated SWS
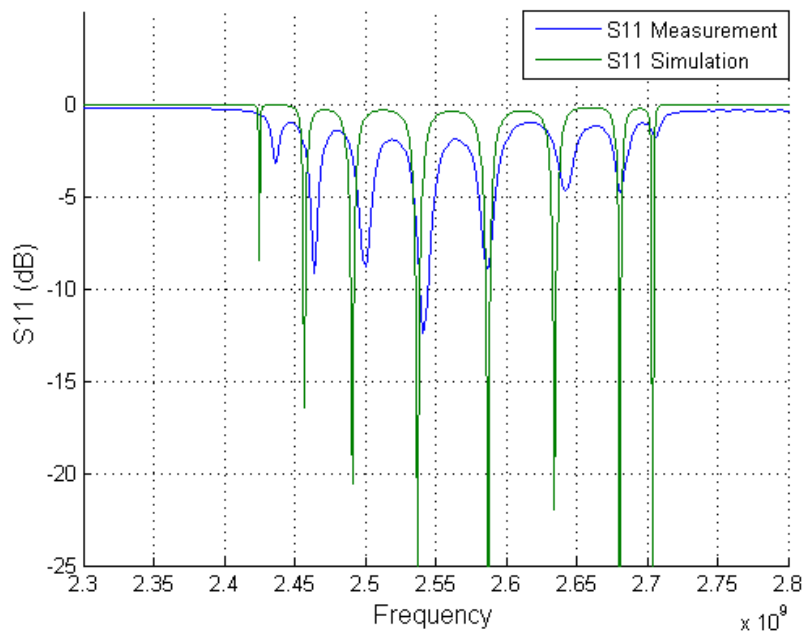
Figure 4.32: S11 of the Fabricated SWS for Mode 3
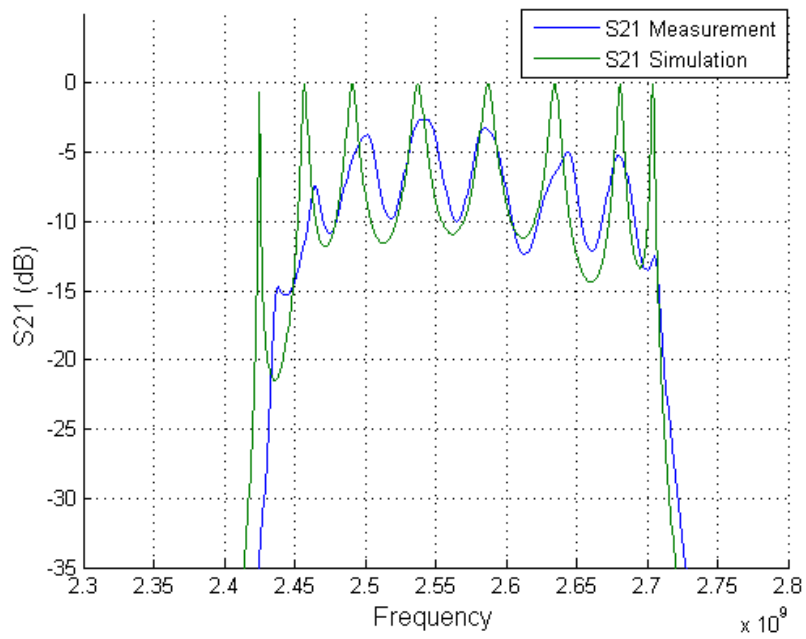
Figure 4.33: S21 of the Fabricated SWS for Mode 3

4.4 Hot Test (PIC Solver) Simulation of SWS

Hot test simulation is performed using the CST Particle-in Cell (PIC) Solver in order to investigate output power, beam parameters and frequency of the RF signal and also validate the proposed SWS. Figure 4.34 shows the proposed the BWO design. The designed BWO consists of 8 unit cell aforementioned above and output guiding part. Output guiding part is circular waveguide with cutoff frequency for TM mode is at 2.1 GHz. The PIC simulation parameters are 450 kV, 100 A electron beam guided by 2T magnetic field. Magnetic field is applied analytically in CST Simulation environment as in Figure 4.35. Magnetic field is used to keep the electron beam moving in the axial direction. SWS part of the BWO composed of 8 unit cell length is 200 mm which corresponds to nearly 1.5λ at 2.4 GHz.
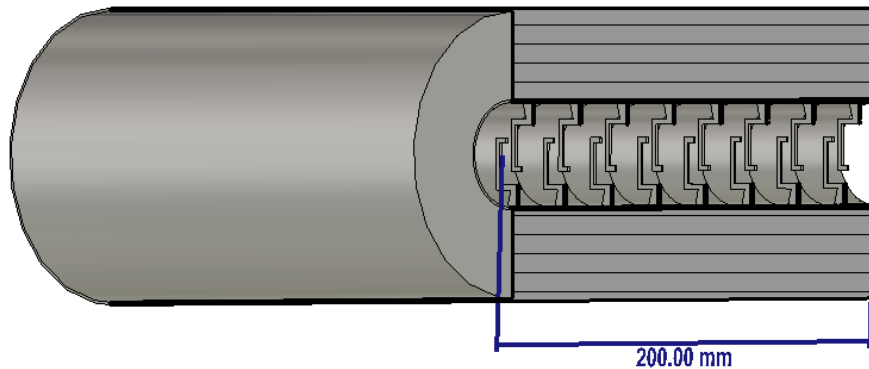
Figure 4.34: Schematic of the BWO

DC annular electron beam with outer radius 5mm and inner radius 2.2 mm is used in hot test simulation since the annular beam has higher space charge limit current and can be better controlled compared to solid beam [91]. So, annular beam is usually adopted by high power microwave sources. Output port is applied at the end of the empty circular waveguide with 55 mm radius. Cut-off frequencies of output guiding part is given in Table 4.3.
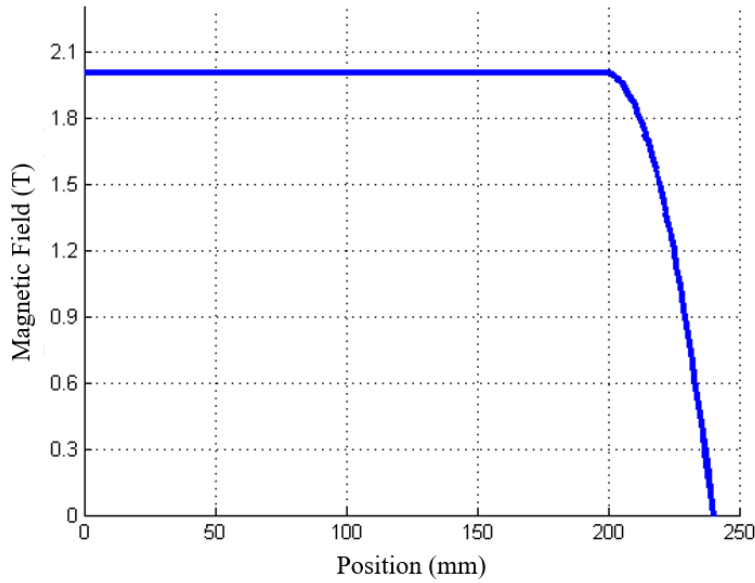
Figure 4.35: Applied Analytical Magnetic Field

Table 4.3: Cutoff frequencies of circular waveguide with 110 mm diameter.

Mode	Cut-off Frequencies
TE_{11}	1.60 GHz
TM_{01}	2.10 GHz
TE_{01}	2.63 GHz

Impedance normalized port voltage is given in Figure 4.36. Mode 3 which is the TM-like mode is the dominant mode. However, mode 1 of the SWS is also excited as expected but not desired. Figure 4.37 shows the other three lowest order modes. Mode 1 is also excited and it decreases the efficiency of BWO. Figure 4.38 shows the electric field of the output at 2.49 GHz. It proves the output electric field is the TM-like mode.

Figure 4.39 shows the Fourier transform of the output signal. Output signal has oscillation at the 2.49 GHz. Output power of the signal for mode 3 is shown in Figure 4.40. Peak power of the signal is 8.3 MW and peak efficiency of the BWO is %18.4
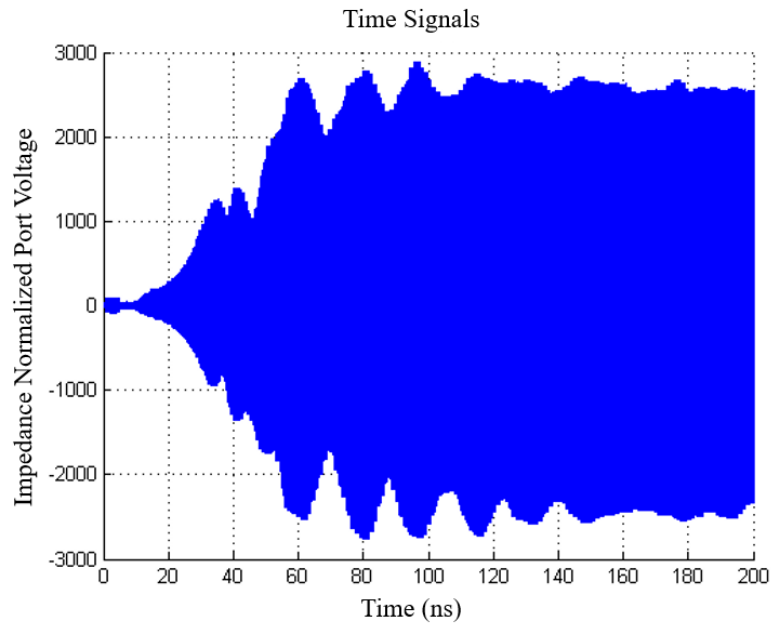
Figure 4.36: Impedance Normalized Output Voltage Signal for Mode 3
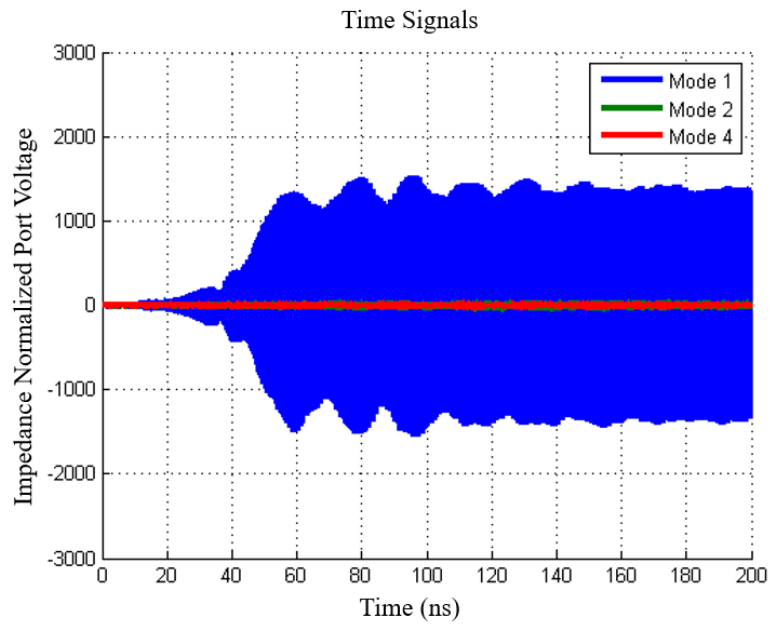
Figure 4.37: Impedance Normalized Output Voltage Signal for Mode 1,2 and 4

59
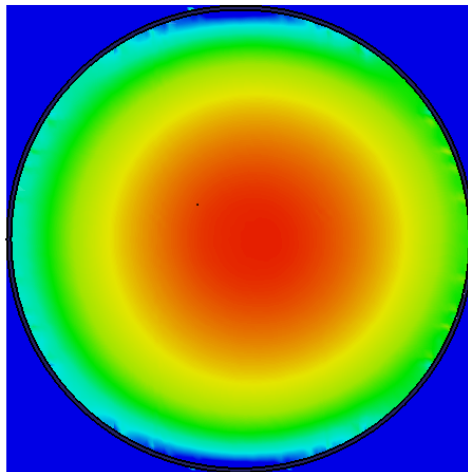
Figure 4.38: Normalized Electric Field at 2.49 GHz

for 450 kV and 100 A. If we add the mode 1 power, efficiency and output power of the BWO are observed as %23.8 and 10.7 MW respectively.
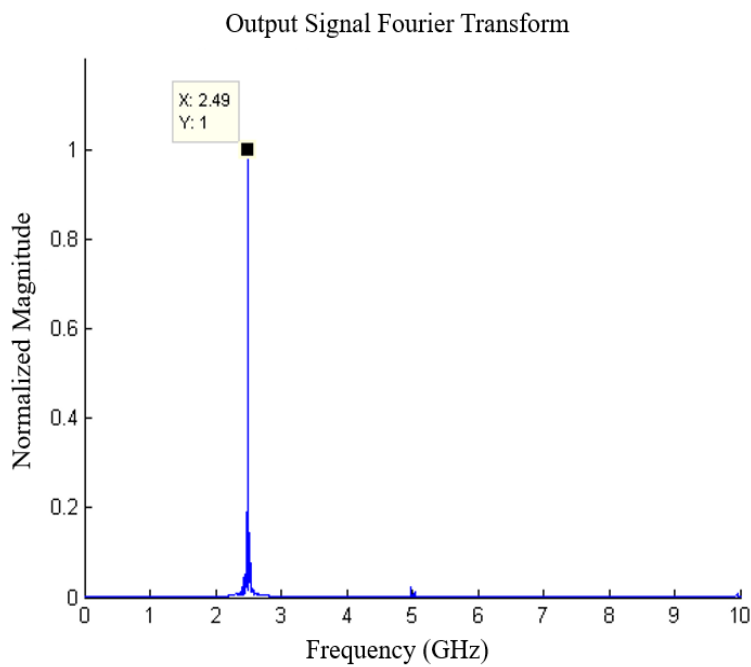
Figure 4.39: Fourier Transform of the Output Signal
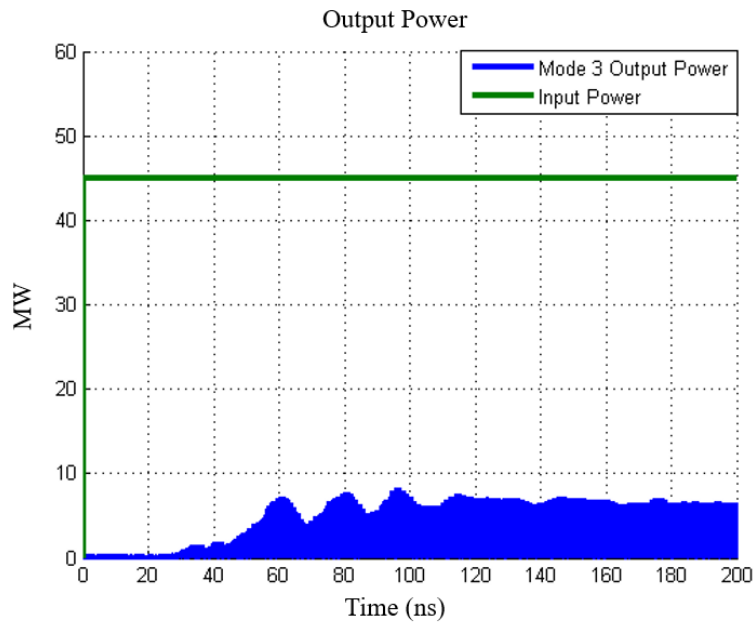
Figure 4.40: Output Power Signal

Figure 4.38 proves that the operation mode is TM like mode. It also shows that proposed SWS can be used for BWO. Also, operation frequency of the mode 3 is in the pass band region of the SWS cold test simulation. Electromagnetic pass band region is between 2.43 - 2.72 GHz for mode 3 as shown in Figure 4.5a. It has correlation between dispersion diagram in Figure 4.5a. Since the BWO is reversed Cherenkov radiation based device, synchronism condition should be provided. Synchronism condition is given in section 3.6. To investigate the synchronism condition, axial component of the electron velocity is observed in phase space plot in Figure 4.41 and Figure 4.42 at 20 ns and 100 ns respectively. In addition to reversed Cherenkov radiation, Cherenkov cyclotron instability should be considered [5]. Synchronism occurs in phase of the wave and the cyclotron motion of the electron particles in a Cherenkov cyclotron instability. To understand the dominant radiation mechanism, magnetic field is decreased to 1 T and simulation is repeated. In this simulation, frequency of the oscillation did not change. Figure 4.43 and Figure 4.44 show the axial velocity of the electron beam under the 1 T analytical magnetic field at 20 ns and 100 ns.

In addition to that Figure 4.45-4.50 show the phase space plot that helps to visualize

61

the energy and the absolute velocity of the particles with respect to position. The PIC phase space plots are observed at t = 20ns, t = 60ns and t = 100 ns.
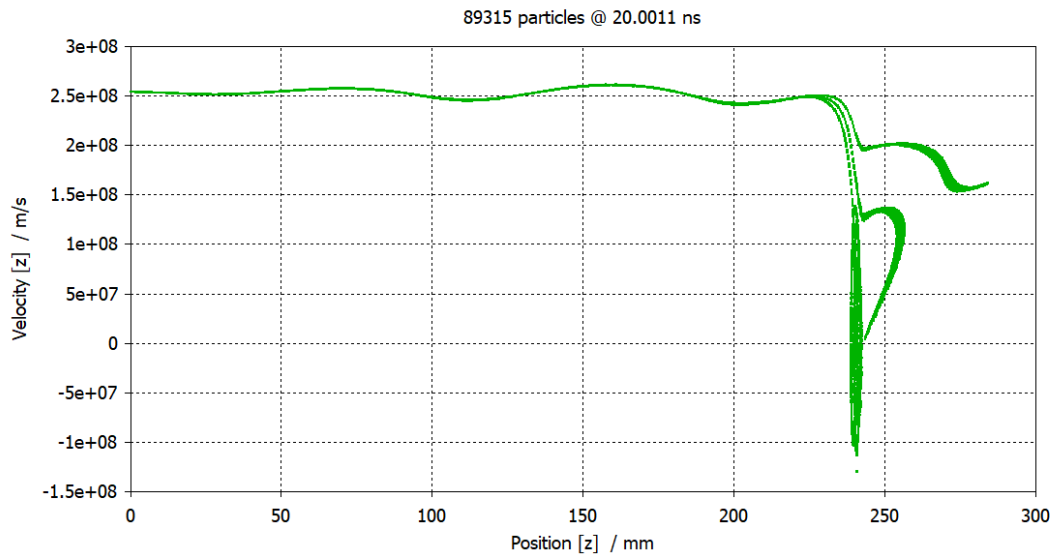
Figure 4.41: Axial Electron Velocity vs. Position at 20 ns
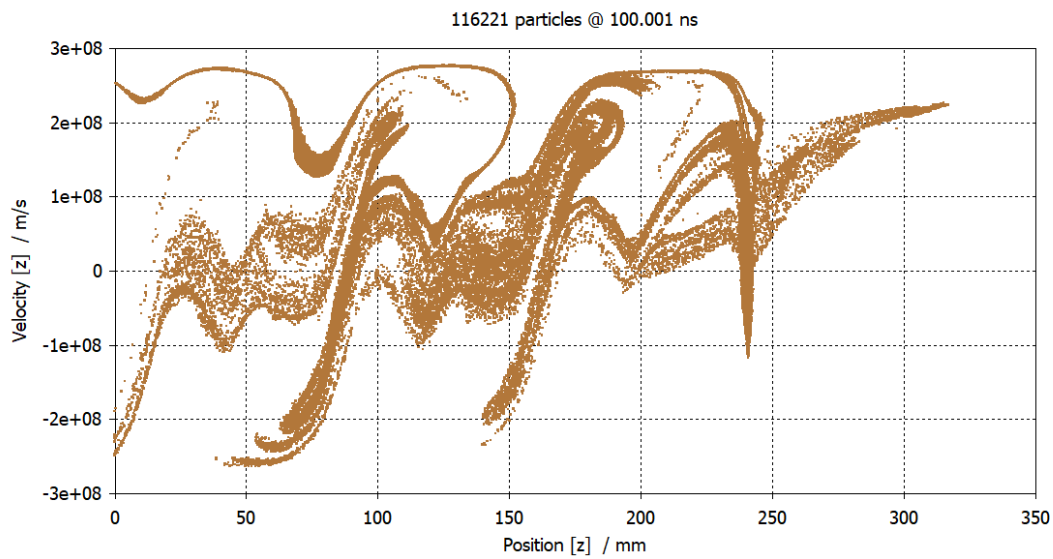
Figure 4.42: Axial Electron Velocity vs. Position at 100 ns
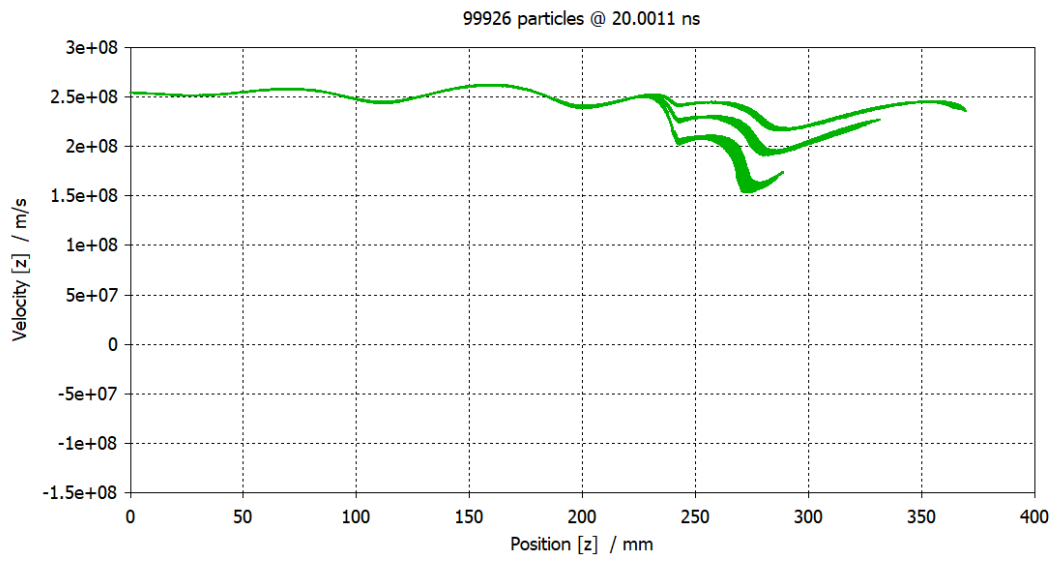
Figure 4.43: Axial Electron Velocity vs. Position at 20 ns for 1 T Magnetic Field
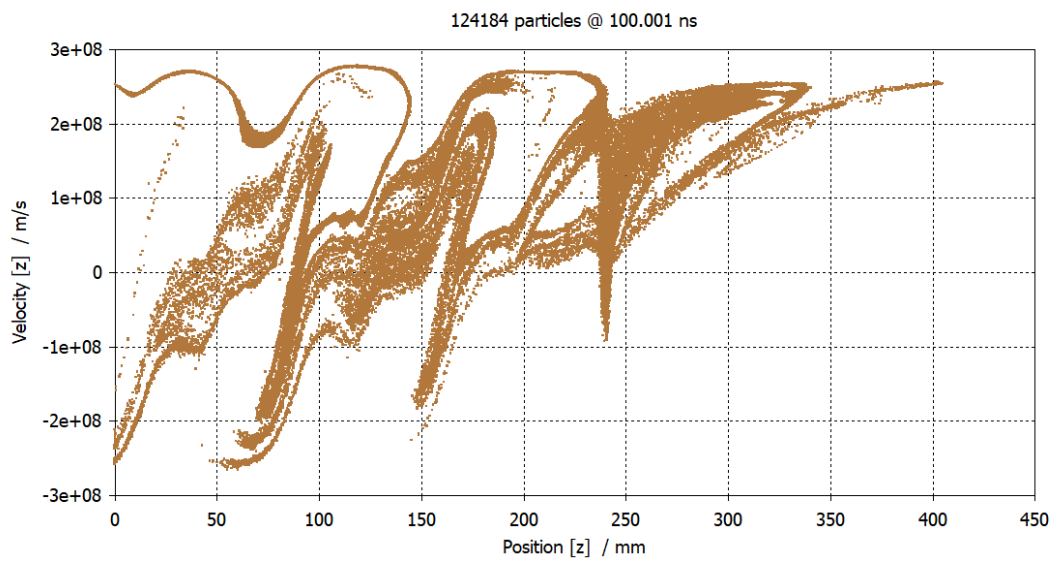
Figure 4.44: Axial Electron Velocity vs. Position at 100 ns for 1 T Magnetic Field

63
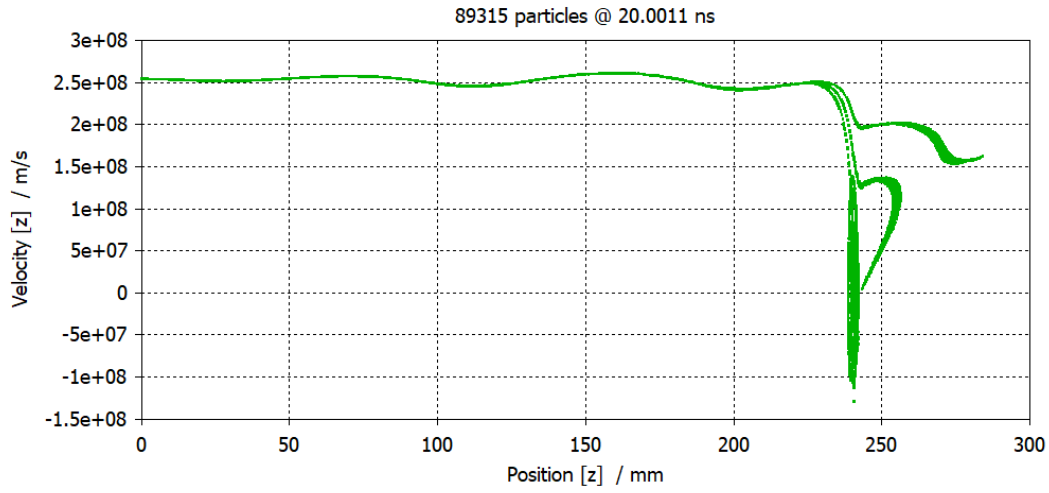
Figure 4.45: Axial Electron Velocity vs. Position at 20 ns
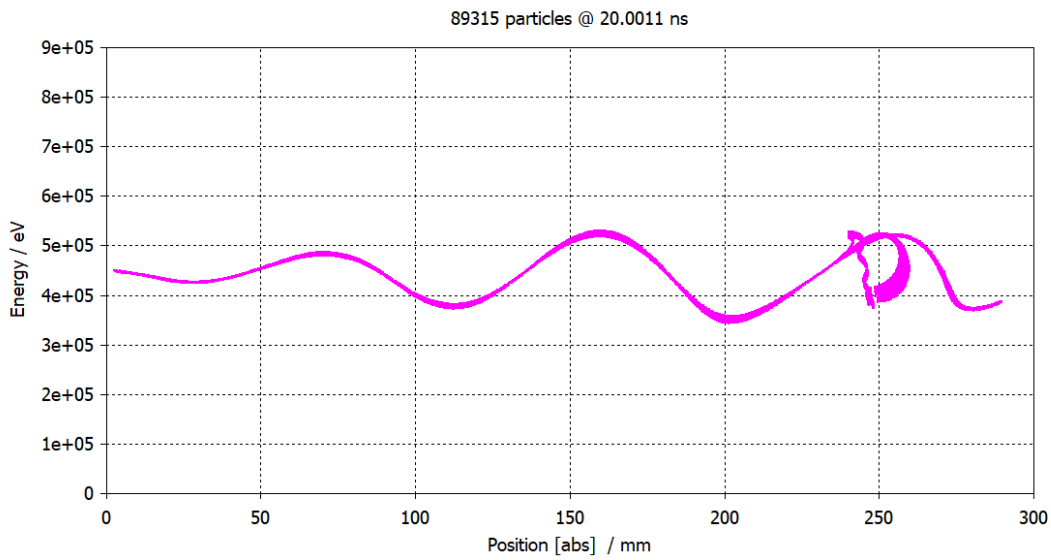
Figure 4.46: Energy of Particles vs. Position at 20 ns

64
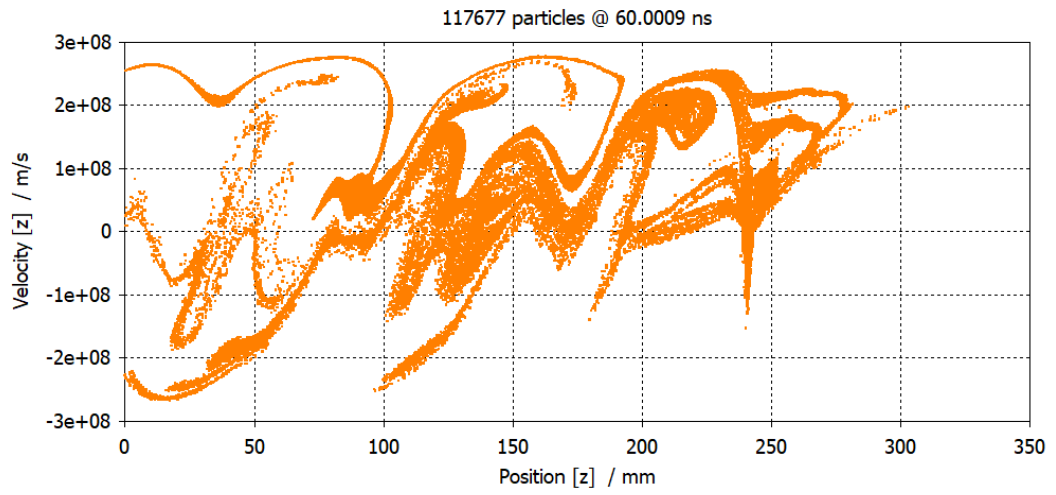
Figure 4.47: Axial Electron Velocity vs. Position at 60 ns
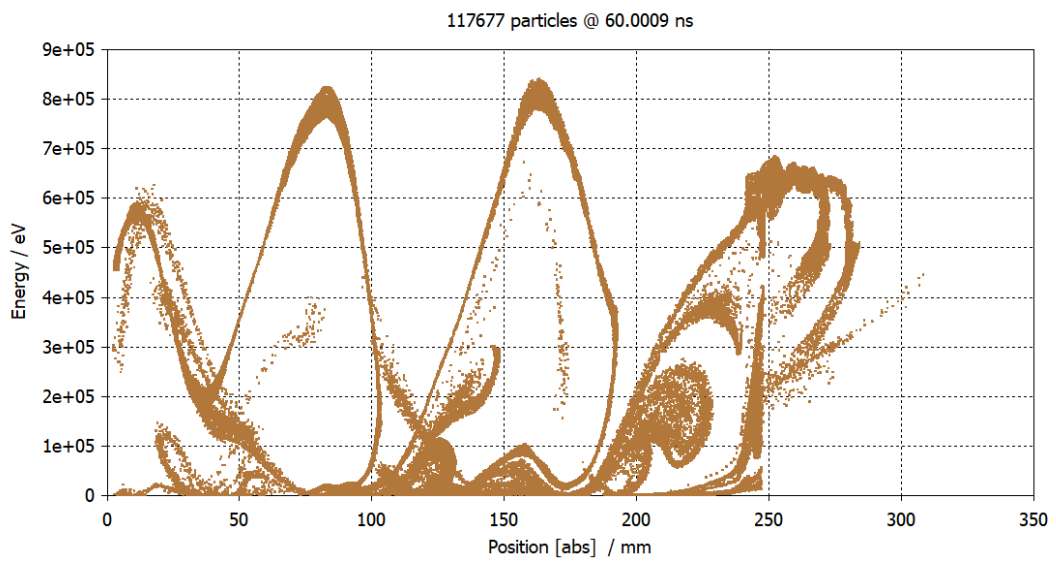
Figure 4.48: Energy of Particles vs. Position at 60 ns
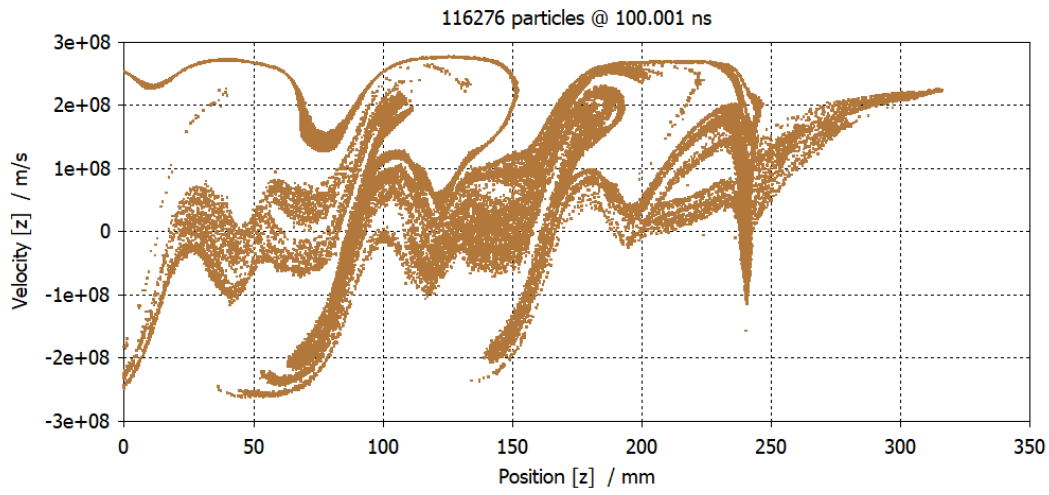
Figure 4.49: Axial Electron Velocity vs. Position at 100 ns
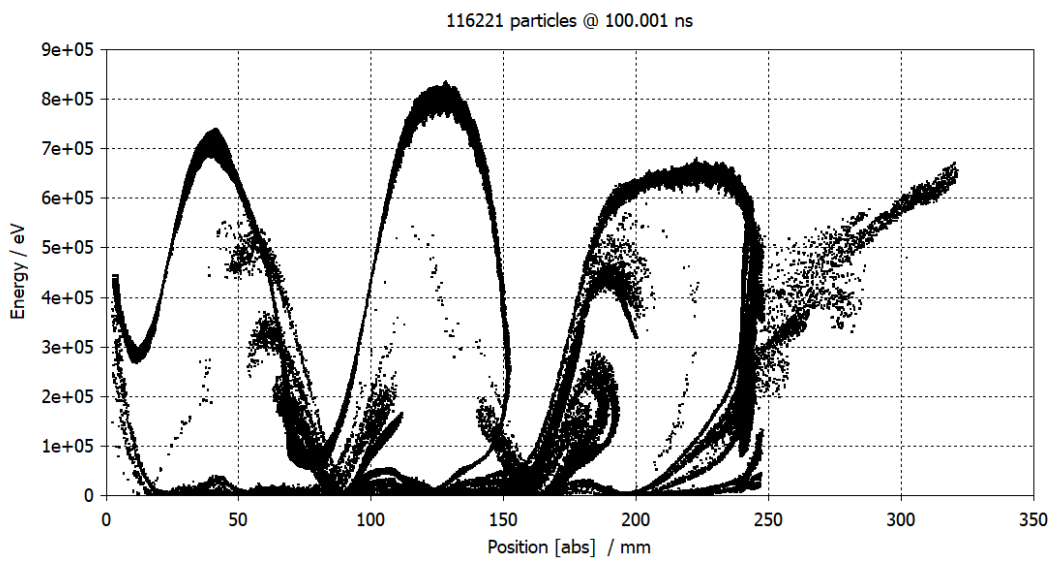
Figure 4.50: Energy of Particles vs. Position at 100 ns

CHAPTER 5

CONCLUSION

Vulnerability of the electronic system has increased in recent years because of the small scale of today's electronic components. Trends on lower voltage and miniaturization continues. In addition, vulnerability of the electronic system is increased because of the use of plastic and composite materials in order to decrease cost instead of metal packaging. As a result of increasing electronic vulnerability, high power microwave weapons is more attractive. The effects of HPM weapons on electronic system can be burnout,upset, jamming and deception. Consequently, research on high power microwave devices has increased in recent years.

Backward wave oscillator (BWO) is the one of the high power microwave devices. BWO composed of electron gun, slow wave structure (SWS) and output coupling part. Operation principle of the BWO is based on beam-wave interaction phenomena. Electron beam is generated in the electron gun part. Electrons transfer their energy to electromagnetic wave in the SWS part. Generally, antenna is used as the coupling part at the end of SWS.

In addition to design of slow wave structure, this thesis includes comprehensive study on works related with high power microwave devices in literature. Chapter 2 is devoted for literature review on high power microwave devices especially backward wave oscillator. It is worth to note that again some researches on BWO. Volakis and his group achieved BWO using 490 kV, 84 A electron beam [51]. They observed 18 MW peak output power. The Schamiloglu group achieved 250 MW output power at 1.4 GHz. They reported the 14% efficiency using 400 kV, 4.5 kA [68]. Researchers at MIT achieved 5.75 MW output power using 500 kV, 84 A electron beam. They reported 14% efficiency at the 2.6 GHz. Besides the backward wave oscillator, work on

travelling wave tube amplifier, klystron and magnetron mentioned briefly. Historical development of these devices is also in the content of the chapter 2.

In this thesis, metamaterial based slow wave structure for backward wave oscillators is analyzed and designed. Novel metamaterial SWS is designed in the 2.43-2.72 GHz frequency range using the dispersion diagram in the commercial software program CST Studio Suite. Dispersion diagram of the unit cell slow wave structure is simulated in Eigen Mode Solver of the CST. Different modes of the SWS is analyzed in the simulation. Since the electrons transfer their energy to axial component of the electromagnetic wave, TM mode is observed as the operation mode. Axial electric field component and absolute electric field is compared to find TM modes on metamaterial slow wave structure. Besides that, interaction impedance is observed in between 10-70 Ω in the 2.45-2.5 GHz. Normalized phase velocity is observed in the interval 0.4-0.6 c in the 2.43-2.6 GHz frequency interval. Group velocity are also investigated in the simulations. Observing the phase velocity and group velocity of the unit cell, backward wave propagation is proved since they are in opposite sign.

To validate the designed unit cell of the slow wave structure, 8 unit cells are combined. Combined 8 unit cells are simulated using the CST Frequency Domain Solver. Combined SWS is fabricated. To observe the TM mode propagation, SWS is excited using the axial pin. Handmade connector is designed to excite the SWS. Using this handmade connector, S11 is observed below the -10 dB in the resonant frequency interval 2.43-2.72 GHz. It is measured in network analyzer in terms of S parameters. Measured slow wave structure is compared with the simulation and SWS is validated observing the passband region in between 2.43-2.72 GHz with correlation of dispersion diagram. Axial pin excitation validates the TM mode propagation in this structure. In addition, using metamaterial significantly decreases the dimension of waveguide for TM mode propagation. Radius of the slow wave structure is 20 mm which is evanescent mode for empty circular waveguide for the 2.42-2.73 GHz.

Finally, operation of backward wave oscillator is investigated. Hot test simulation is also accomplished in CST Particle Studio. In this simulation, annular electron beam with 5 mm outer radius and 2.2 mm inner radius is defined using the DC electron emission model. 450 kV, 100 A electron beam is used for this simulation. To guide

68

the beam, 2 T theoretical magnetic field is applied in the axial direction. It was validated that SWS is suitable for TM mode propagation in the cold test simulation. As expected, mode 3 output is observed which is TM-like mode at the output port. 10.7 MW output power is achieved with 23.8 % efficiency at the 2.49 GHz. Simulation time is 200 ns and stable power is observed after the first 60 ns. Phase space plots are also observed to investigate the electron motion and energy. Simulation tools are crucial in charged particle problems. It should include the motion of electrons and interaction of electrons with electromagnetic waves. In order to simulate these problems, particle-in-cell codes should be used. Besides that, frequency domain solver, time domain solver, eigen mode solver are used in simulation.

High power microwave devices include several sections that are prime power, pulsed power and microwave part. It is not easy task to verify the designed structure in experiment. It requires interdisciplinary work. Cold test validation of the microwave part is investigated with both simulation and measurement in this thesis. Hot test experiment will be subject of the future work. Electron gun should be designed for hot test simulation. Hot test simulation may be considered for higher current in order to increase efficiency. Efficiency may also be increased optimizing the slot distance between metamaterial units. Slow wave structure may be used for other microwave parts such as filters.

REFERENCES

[1] J. Benford, J. A. Swegle and E. Schamiloglu, High Power Microwaves, Boca Raton, FL: CRC Press, pp.281-285, 2015.

[2] L.Schacter, Beam-Wave Interaction in Periodic and Quasi-Periodic Structures, New York:Springer,2011

[3] Pozar David M. , Microwave Engineering, John Wiley & Sons, Inc, Year: 2012

[4] A.N. Vlasov, A.S.Ilyin, and Y.Carmel, "Cyclotron effects in relativistic backward-wave oscillators operating at low magnetic fields", IEEE Trans. Plasma Sci., vol. 26, no. 3, pp. 605–614, Jun. 1998.

[5] J. S. Hummelt, X. Lu, H. Xu, I. Mastovsky, M. A. Shapiro, and R.J.Temkin, "Coherent Cherenkov-cyclotron radiation excited by an electron beam in a metamaterial waveguide", Phys. Rev. Lett. 117(23), 237701 (2016).

[6] Duan, Z., X. Tang, Z. Wang, et al., "Observation of the Reversed Cherenkov Radiation", Nature Communications, vol. 8, 14901, 2017.

[7] Chuan Sheng Liu and V. K. Tripathi, "Stimulated coherent Smith-Purcell radiation from a metallic grating," in IEEE Journal of Quantum Electronics, vol. 35, no. 10, pp. 1386-1389, Oct. 1999

[8] E. M. Totmeninov, A. I. Klimov and V. V. Rostov, "Relativistic Cherenkov Microwave Oscillator Without a Guiding Magnetic Field," in IEEE Transactions on Plasma Science, vol. 37, no. 7, pp. 1242-1245, July 2009

[9] http://www.boeing.com/Features/2012/10/bds_champ_10_22_12.html, 2018.

[10] http://www.claws.in/1616/27-jul-2016-%E2%80%93-resurgence-of-high-power-microwave-weapons-sanatan-kulshrestha.html,2018

[11] Sarkar, T. K.; Mailloux, Robert; Oliner, Arthur A. (2006). "History of Wireless" . John Wiley and Sons. pp. 215–228

[12] M. Franzi, R. M. Gilgenbach, B. Hoff , G. Greening, Y. Y. Lau, N. M.Jordan, D. Simon, D. French, and J. Luginsland, "Coaxial all cavity extraction in the recirculating planar magnetron," IEEE International Vacuum Electronics Conference, pp. 89-90, April 2014.

[13] M. A. Franzi, R. M. Gilgenbach, B. W. Hoff, D. A. Chalenski, D. Simon,Y. Y. Lau, and J. Luginsland, "Recirculating-Planar-Magnetron Simulations and experiment," IEEE Transactions on Plasma Science, vol. 41, no. 4, April 2013.

[14] M. Franzi, R. M. Gilgenbach, D. M. French, B. W. Hoff, Y. Y. Lau, D.Simon, and J. W. Luginsland, "Recirculating Planar Magnetron modeling and experiments," 2011 Abstracts IEEE International Conference on Plasma Science, pp. 1-1, Chicago, IL, 2011.

[15] R. M. Gilgenbach, Y. Y. Lau, D. M. French, B. W. Hoff, M. Franzi and J. Luginsland, "Recirculating Planar Magnetrons for High-Power High- Frequency Radiation Generation," IEEE Transactions on Plasma Science, vol. 39, no. 4, pp. 980-987, April 2011.

[16] F. Hamamah, W. F. H. W. Ahmad, C. Gomes, M. M. Isa and M. J. Homam, "High power microwave devices: Development since 1880," 2017 IEEE Asia Pacific Microwave Conference (APMC), Kuala Lumpar, 2017, pp. 825-828.

[17] N. M. Jordan, G. B. Greening, S. C. Exelby, R. M. Gilgenbach, Y. Y.Lau, and B. W. Hoff, "Additively manufactured anodes in a relativistic Planar Magnetron," IEEE International Vacuum Electronics Conference (IVEC), pp. 1-2, Monterey, CA, 2016

[18] W. Dong, Q. Fen, C. Daibing, W Jie, Z. Xinkai, and A. Haishi, "Particle simulation and experimental research on L-band double ladder cathode MILO," High Power Laser and Particle Beams, vol 4, no 040, 2010.

[19] Z. Qi, J. Zhang, H. Zhong, Q. Zhang, and D. Zhu, "An improved suppression method of the transverse-electromagnetic mode leakage with two reflectors in the triaxial klystron amplifier," Physics of Plasmas, vol. 21, issue. 7, no. 073103, 2014.

[20] R. Xiao, Y. Deng, C. Chen, J. Sun, X. Zhang, and L. Zhang, "A highpower high-efficiency klystron like relativistic backward wave oscillator with a dual-cavity extractor," Northwest Institute of Nuclear Technology Xi'an, Shaanxi Province, China, Applied Physics Letters, vol. 98,issue .10, no. 101502, 2011.

[21] G. Caryotakis, "The klystron: A microwave source of surprising range and endurance," Phys. Plasmas, vol. 5, no. 5, p. 1590, 1998.

[22] S. S. H. Gold, G. S. Nusinovich, "Review of high-power microwave source research," Rev. Sci. Instrum. 68 (1997) 3945–3974.

[23] G. S. Nusinovich, T. M. Antonsen, Jr., V. L. Bratman, and N. S. Ginzburg,in Applications of High-Power Microwaves, edited by A. V. Gaponov-Grekhov and V. L. Granatstein Artech House, Boston, 1994!,Chap. 2.

[24] Lingwood, C. J. (2010). High power high efficiency multiple-beam klystron design (Order No. 10022217). Available from ProQuest Dissertations & Theses Global. (1774213072). Retrieved from url-https://search.proquest.com/docview/1774213072?accountid=13014

[25] Ł3 electron devices "High-Power Klystron" L5859 datasheet,Mar.2016 Available: urlhttps://www2.l3t.com/edd/pdfs/datasheets/5859.pdf

[26] A. Yano, S.Miyake, S. Kazakov, A. Larionov, V. Teriaev, and Y. H. Chin.The Toshiba E3736 multi-beam klystron. In LINAC 2004, pages 706–708,Lübeck, Germany, May 2004.

[27] Thales Electron Devices. Thales TH2162 Klystron Datasheet https://www.thalesgroup.com/sites/default/files/database/d7/asset/document/TH2162.pdf

[28] M. Read, R. Jackson, P. Ferguson, G. Nusinovich and R. L. Ives, "Design of a 10 MW,L-Band, Annular Beam Klystron," in IEEE Transactions on Electron Devices, vol. 61, no. 6, pp. 1836-1841, June 2014.

[29] Z. Qi, J. Zhang, Q. Zhang, H. Zhong, L. Xu and L. Yang, "Design and Experimental Demonstration of a Long-Pulse, X-Band Triaxial Klystron Amplifier With an Asymmetric Input Cavity," in IEEE Electron Device Letters, vol. 37, no. 6, pp. 782-784, June 2016.

[30] S. Chen et al., "Particle-in-Cell Simulation and Optimization of Multigap Extended Output Cavity for a W-Band Sheet-Beam EIK," in IEEE Transactions on Plasma Science, vol. 42, no. 1, pp. 91-98, Jan. 2014.

[31] G. B. Collins, Microwave Magnetrons. New York: McGraw-Hill, 1948.

[32] Dr. Monika Balk, Seung-Won Baek "A Multiphysics Approach to Magnetron and Microwave Oven Design", CST AG, Germany 2013

[33] "Ł3 electron devices product catalogue. [Online]. Available: url https://www2.l3t.com/edd/products/magnetrons.htm

[34] "Toshiba product catalogue." [Online]. Available: url http://www.hokuto.co.jp/eng/products/magnetron/list.htm

[35] "GLVAC product catalogue." [Online]. Available: url http://www.hokuto.co.jp/eng/products/magnetron/list.htm

[36] S. Khatoon, R. P. Yadav and A. Jain, "Design and Simulation of 8-cavity hole-slot type magnetron in CST," 2018 2nd International Conference on Electronics, Materials Engineering & Nano-Technology (IEMENTech), Kolkata, 2018, pp. 1-5.

[37] T. Isenlik and K. Yegin, "Tutorial on the Design of Hole-Slot-Type Cavity Magnetron Using CST Particle Studio," in IEEE Transactions on Plasma Science, vol. 41, no. 2, pp. 296-304, Feb. 2013.

[38] A. Sayapin, A. Levin and Y. E. Krasik, "Stabilization of the Frequency of Relativistic S-Band Magnetron With Radial Output," in IEEE Transactions on Plasma Science, vol. 41, no. 10, pp. 3001-3004, Oct. 2013.

[39] Z. Liu, X. Chen, M. Yang, K. Huang and C. Liu, "Experimental Studies on a 1-kW High-Gain S-Band Magnetron Amplifier With Output Phase Control Based on Load–Pull Characterization," in IEEE Transactions on Plasma Science, vol. 46, no. 4, pp. 909-916, April 2018.

[40] B. Yang, T. Mitani and N. Shinohara, "Development of a 5.8 GHz power-variable phase-controlled magnetron," 2017 Eighteenth International Vacuum Electronics Conference (IVEC), London, 2017, pp. 1-2

[41] Traveling-wave tube, "Encyclopædia Britannica " November 25, 2018 urlhttps://www.britannica.com/technology/traveling-wave-tube/media/603591/138

[42] "Ł3 electron devices product catalogue." [Online]. Available: https://www2.l3t.com/edd/products/twt_hp2.htm

[43] " Communications & Power Industries (CPI)" [Online]. Available: url-https://www.cpii.com/product.cfm/1/19/129

[44] A. S. Gilmour," Klstrons,Traveling Wave Tubes, Magnetrons, Crossed-Field Amplifiers, and Gyrotrons," Artech House, pp.317 , 2015.

[45] R. Kompfner, "The Invention of Traveling Wave Tube," IEEE Trans. Electron Dev., vol. ED-23, p. 730, 1976.

[46] H. R. Johnson, "Backward-Wave Oscillators," in Proceedings of the IRE, vol. 43, no. 6, pp. 684-697, June 1955.

[47] J.A. Nation, "On the Coupling of a High-Current Relativistic Electron Beam to a Slow Wave Structure," Appl. Phys. Lett., vol. 17, p. 491, 1970.

[48] R. A. Kehs et al., "A High-Power Backward-Wave Oscillator Driven by a Relativistic Electron Beam," in IEEE Transactions on Plasma Science, vol. 13, no. 6, pp. 559-562, Dec. 1985.

[49] Swegle, J. A., Poukey, J. W., & Leifeste, G. T. (1985). "Backward wave oscillators with rippled wall resonators: Analytic theory and numerical simulation." Physics of Fluids, 28(9), 2882–2894.

[50] Diana Gamzina, Diana Gamzina, Xiang Li, Xiang Li, Christian Hurd, Christian Hurd, Ye Tang, Ye Tang, Xuejiao Huang, Xuejiao Huang, Yuan Zheng, Yuan Zheng, Logan Himes, Logan Himes, Michelle Gonzalez, Michelle Gonzalez, Hanyan Li, Hanyan Li, Pan Pan, Pan Pan, Rosa Letizia, Rosa Letizia, Jinjun Feng, Jinjun Feng, Neville C. Luhmann, Neville C. Luhmann, Claudio Paoloni, Claudio Paoloni, "Backward wave oscillator for high power generation at THz frequencies", Proc. SPIE 10383, Terahertz Emitters, Receivers, and Applications VIII, 1038303 (23 August 2017);

[51] U. Chipengo, N. K. Nahar and J. L. Volakis, "Backward-Wave Oscillator Operating in Low Magnetic Fields Using a Hybrid-TE$_{11}$ Mode," in IEEE Transactions on Electron Devices, vol. 64, no. 9, pp. 3863-3869, Sept. 2017.

[52] B. Levush, T. M. Antonsen, A. Bromborsky, W. -. Lou and Y. Carmel, "Theory of relativistic backward-wave oscillators with end reflectors," in IEEE Transactions on Plasma Science, vol. 20, no. 3, pp. 263-280, June 1992.

[53] L. D. Moreland et al., "Efficiency enhancement of high power vacuum BWO's using nonuniform slow wave structures," in IEEE Transactions on Plasma Science, vol. 22, no. 5, pp. 554-565, Oct. 1994.

[54] D. K. Abe et al., "Experimental studies of overmoded relativistic backward-wave oscillators," in IEEE Transactions on Plasma Science, vol. 26, no. 3, pp. 591-604, June 1998.

[55] Amin MR, Ogura K, Kojima J, Sagor RH. Electromagnetic properties of a trapezoidally corrugated slow wave structure for backward wave oscillators. IEEE Transactions on Plasma Science. 2014;42(6):1495-1501

[56] Jun Zhang, Hui-Huang Zhong and Ling Luo, "A novel overmoded slow-wave high-power microwave (HPM) Generator," in IEEE Transactions on Plasma Science, vol. 32, no. 6, pp. 2236-2242, Dec. 2004.

[57] M. Mineo and C. Paoloni, "Double-Corrugated Rectangular Waveguide Slow-Wave Structure for Terahertz Vacuum Devices," in IEEE Transactions on Electron Devices, vol. 57, no. 11, pp. 3169-3175, Nov. 2010.

[58] L. Yue, J. Huang, G. Wu, Y. Wei, W. Wang and Y. Gong, "Reentrant double-staggered ladder coupled-cavity structure for X-band traveling-wave tube," 2017 Eighteenth International Vacuum Electronics Conference (IVEC), London, 2017, pp. 1-2.

[59] S. C. Yurt, A. Elfrgani, M. I. Fuks, K. Ilyenko and E. Schamiloglu, "Similarity of Properties of Metamaterial Slow-Wave Structures and Metallic Periodic Structures," in IEEE Transactions on Plasma Science, vol. 44, no. 8, pp. 1280-1286, Aug. 2016.

76

[60] V. G. Veselago, "The electrodynamics of substances with simultaneously negative values ϵ of and μ," Sov. Phys.—Usp., vol. 10, no. 4,pp. 509–514, 1968.

[61] Z. Y. Duan, B.-I. Wu, J. Lu, J. A. Kong, and M. Chen, "Cherenkov radiation in anisotropic double negative metamaterials," Opt. Express 16, 18479 (2008).

[62] Z. Duan et al., "Review of metamaterial-inspired vacuum electron devices," 2018 IEEE International Vacuum Electronics Conference (IVEC), Monterey, CA, 2018, pp. 29-30.

[63] Hummelt, J.S., S.M.Lewis,M.A.Shapiro, *et al.*, " Design of a Metamaterial-Based Backward-Wave Oscillator,"IEEE Transactions on Plasma Science, vol 42, no4, pp930-936,2014

[64] Hummelt, J.S., X.Lu, H. Xu, *et al.*, " Coherent Cherenkov-Cyclotron Radiation Excited by an Electron Beam in a Metamaterial Waveguide" Physical Review Letters, vol. 117, no. 23,237701, 2016.

[65] G. S. Nusinovich, "Introduction to the Physics of Gyrotrons," 1st ed. (John Hopkins University Press, Baltimore, MD,2004).

[66] Xueying.Lu, Jacob C. Stephens, *et al.*, "High Power long pulse microwave generation from metamaterial structure with reverse symmetry" Physics of plasmas 25,023102 (2018).

[67] S. Prasad et al., "A compact high-power microwave metamaterial slow-wave structure: From computational design to hot test validation," 2017 Computing and Electromagnetics International Workshop (CEM), Barcelona, 2017, pp. 61-62.

[68] S. C. Yurt, S. Prasad, M. Fuks and E. Schamiloglu, "Designing of an O-type BWO with a metamaterial slow-wave structure," 2016 IEEE International Vacuum Electronics Conference (IVEC), Monterey, CA, 2016, pp. 1-2.

[69] Duan,Z., J.S. Hummelt, M.A.Shapiro, *et al.*, "Subwavelength Waveguide Loaded by Complementary Electric Metamaterial for Vacuum Electron Devices," Physics of Plasmas, vol.21, no 10, 103301.2014

77

[70] Wang.Y., Z. Duan, X.Tang, *et al.*, "All-metal Metamaterial Slow-Wave Structure for High Power Sources with High Efficiency," Applied Physics Letters, vol. 107, no. 15, 153502, 2015

[71] Y. Wang et al., "S-Band High-Efficiency Metamaterial Microwave Sources," in IEEE Transactions on Electron Devices, vol. 63, no. 9, pp. 3747-3752, Sept. 2016.

[72] Duan,Z.,X.Tang, Z. Wang, *et al.*, "Observation of the Reversed Cherenkov Radiation," Nature Communications, vol 8, 14901,2017

[73] G.Shvets "Photonic Approach to Making a Material with a Negative Index of Refraction", Phys. Rev. B, vol 67. 035109, 2003

[74] H. Guo, Y. Cannel, W.R. Lou, L. Chen, J. Rodgers, D.K. Abe, A. Bromborsky, W.Destler, and V.L. Granatstein, "A Novel Highly Accurate Synthetic Technique for Determination of the Dispersive Characteristics in Periodic Slow Wave Circuits," IEEE Trans. Microw. Theory Techn., vol. MTT-40, pp. 2086-2094, 1992.

[75] U. Chipengo, N. K. Nahar and J. L. Volakis, "Cold Test Validation of Novel Slow Wave Structure for High-Power Backward-Wave Oscillators," in IEEE Transactions on Plasma Science, vol. 44, no. 6, pp. 911-917, June 2016.

[76] Shulim E. Tsimring, Electron Beams and Microwave Vacuum Electronic. New Jersey: Wiley, 2007, pp. 297-298.

[77] Crowell, C. R. (1965). "The Richardson constant for thermionic emission in Schottky barrier diodes". Solid-State Electronics. 8 (4): 395–399

[78] S. Humphries, Charged Particle Beams. New Mexico: Field Precision, 2002

[79] Cerenkov, P. A. "Visible emission of clean liquids by action of g radiation". Dokl.Akad. Nauk SSSR 2, 451–454 (1934).

[80] T. H. Kho and A. T. Lin, "Cyclotron-Cherenkov and Cherenkov instabilities," in IEEE Transactions on Plasma Science, vol. 18, no. 3, pp. 513-517, June 1990.

[81] G. S. Nusinovich and D. Zhao, "Combined Resonances in Cyclotron Masers With Periodic Slow-Wave Structures," in IEEE Transactions on Plasma Science, vol. 43, no. 3, pp. 804-814, March 2015.

[82] J. B. Pendry, A. J. Holden, D. J. Robbins and W. J. Stewart, "Magnetism from conductors and enhanced nonlinear phenomena," IEEE Transactions on Microwave Theory and Techniques, vol. 47, no. 11, pp. 2075-2084, 1999.

[83] D. R. Smith, W. J. Padilla, D. C. Vier, S. C. Nemat-Nasser and S. Schultz,"Composite Medium with Simultaneously Negative Permeability and Permittivity," Physical Review letters, vol. 84, no. 18, pp. 4185-4187, 2000.

[84] D. R. Smith and N. Kroll, "Negative Refractive Index in Left-Handed Materials,"Physical Review Letters, vol. 85, no. 14, pp. 2933-2936, 2000.

[85] D. R. Smith, D. C. Vier, T. Koschny and a. C. M. Soukoulis, "Electromagnetic parameter retrieval from inhomogeneous metamaterials," Physical Review E, vol. 71,pp. 0366171- 03661711, 2005.

[86] Z. Szabó, G.-H. Park, R. Hedge and E.-P. Li, "A Unique Extraction of Metamaterial Parameters Based on Kramers–Kronig Relationship," IEEE Transactions on Microwave Theory and Techniques, vol. 58, no. 10, pp. 2646-2653, 2010.

[87] (2018). CST Studio Suite . Computer Simulation Technologies. [Online]. Available: https://www.cst.com/products/csts2 (Last accessed on December, 2018)

[88] M. Zuboraj, U. Chipengo, N. K. Nahar and J. L. Volakis, "Experimental Validation of Slow-Wave Phenomena in Curved Ring-Bar Slow-Wave Structure," in IEEE Transactions on Plasma Science, vol. 44, no. 9, pp. 1794-1799, Sept. 2016

[89] H. Guo et al., "A novel highly accurate synthetic technique for determination of the dispersive characteristics in periodic slow wave circuits," in IEEE Transactions on Microwave Theory and Techniques, vol. 40, no. 11, pp. 2086-2094, Nov. 1992.

[90] U. Chipengo, N. K. Nahar and J. L. Volakis, "Cold Test Validation of Novel Slow Wave Structure for High-Power Backward-Wave Oscillators," in IEEE Transactions on Plasma Science, vol. 44, no. 6, pp. 911-917, June 2016.

[91] Dai,Ouzhixiong and He,Juntao and Ling,Junpu and Wang,Lei and Han,Jianxun, "A novel L-band slow wave structure for compact and high-efficiency relativistic Cerenkov oscillator," in Physics of Plasmas, vol.25, no 9, pp. 93-103, 2018

[92] J. H. Booske et al., "Accurate parametric modeling of folded waveguide circuits for millimeter-wave traveling wave tubes," in IEEE Transactions on Electron Devices, vol. 52, no. 5, pp. 685-694, May 2005.